LAST LAYER RE-TRAINING IS SUFFICIENT FOR ROBUSTNESS TO SPURIOUS CORRELATIONS

Anonymous authors
Paper under double-blind review

ABSTRACT

Neural network classifiers can largely rely on simple spurious features, such as backgrounds, to make predictions. However, even in these cases, we show that they still often learn core features associated with the desired attributes of the data, contrary to recent findings. Inspired by this insight, we demonstrate that simple last layer retraining can match or outperform state-of-the-art approaches on spurious correlation benchmarks, but with profoundly lower complexity and computational expenses. Moreover, we show that last layer retraining on large ImageNet-trained models can also significantly reduce reliance on background and texture information, improving robustness to covariate shift, after only minutes of training on a single GPU.

1 INTRODUCTION

Realistic datasets in deep learning are riddled with *spurious correlations* — patterns that are predictive of the target in the train data, but that are irrelevant to the true labeling function. For example, most of the images labeled as butterfly on ImageNet also show flowers (Singla & Feizi, 2021), and most of the images labeled as tench show a fisherman holding the tench (Brendel & Bethge, 2019). Deep neural networks rely on these spurious features, and consequently degrade in performance when tested on datapoints where the spurious correlations break, for example, on images with unusual background contexts (Geirhos et al., 2020; Rosenfeld et al., 2018; Beery et al., 2018). In an especially alarming example, CNNs trained to recognize pneumonia were shown to rely on hospital-specific metal tokens in the chest X-ray scans, instead of features relevant to pneumonia (Zech et al., 2018).

In this paper, we investigate what features are in fact learned on datasets with spurious correlations. We find that even when neural networks appear to heavily rely on spurious features and perform poorly on minority groups where the spurious correlation is broken, they still learn the core features sufficiently well. These core features, associated with the semantic structure of the problem, are learned even in cases when the spurious features are much simpler than the core features (see Section 4.2) and in some cases even when no minority group examples are present in the training data! While both the relevant and spurious features are learned, the spurious features can be highly weighted in the final classification layer of the model, leading to poor predictions on the minority groups.

Inspired by these observations, we propose *Deep Feature Reweighting* (DFR), a simple and effective method for improving worst-group accuracy of neural network classifiers in the presence of spurious features. We illustrate DFR in Figure 1. In DFR, we simply retrain the last layer of a classification model trained with standard Empirical Risk Minimization (ERM), using a small set of *reweighting* data where the spurious correlation does not hold. DFR achieves state-of-the-art performance on popular spurious correlation benchmarks by simply reweighting the features of a trained ERM classifier, with no need to re-train the feature extractor. Moreover, we show that DFR can be used to reduce reliance on background and texture information and improve robustness to certain types of covariate shift in large-scale models trained on ImageNet, by simply retraining the last layer of these models. We note that the reason DFR can be so successful is because standard neural networks *are* in fact learning core features, even if they do not primarily rely on these features to make predictions, contrary to recent findings (Hermann & Lampinen, 2020; Shah et al., 2020). Since DFR only requires retraining a last layer, amounting to logistic regression, it is extremely simple, easy to tune and computationally inexpensive relative to the alternatives, yet can provide state-of-the-art performance. Indeed, DFR can reduce texture bias and improve robustness of large ImageNet trained models, in only minutes on a single GPU.

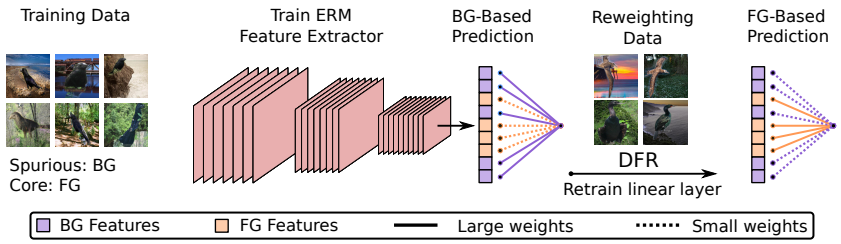

Figure 1: **Deep feature reweighting (DFR).** An illustration of the DFR method on the Waterbirds dataset, where the background (BG) is spuriously correlated with the foreground (FG). Standard ERM classifiers learn both features relevant to the background and the foreground, and weight them in a way that the model performs poorly on images with confusing backgrounds. With DFR, we simply reweight these features by retraining the last linear layer on a small dataset where the backgrounds are not spuriously correlated with the foreground. The resulting DFR model primarily relies on the foreground, and performs much better on images with confusing backgrounds.

2 Problem Setting

We consider classification problems, where we assume that the data consists of several *groups* $\mathcal{G}_i$, which are often defined by a combination of a label and spurious attribute. Each group has its own data distribution $p_i(x, y)$, and the training data distribution is a mixture of the group distributions $p(x, y) = \sum_i \alpha_i p_i(x, y)$, where α_i is the proportion of group $\mathcal{G}_i$ in the data. For example, in the Waterbirds dataset (Sagawa et al., 2019), the task is to classify whether an image shows a landbird or a waterbird. The groups correspond to images of waterbirds on water background ($\mathcal{G}_1$), waterbirds on land background ($\mathcal{G}_2$), landbirds on water background ($\mathcal{G}_3$) and landbirds on land background ($\mathcal{G}_4$). See Figure 6 for a visual description of the Waterbirds data. We will consider the scenario when the groups are not equally represented in the data: for example, on Waterbirds the sizes of the groups are 3498, 184, 56 and 1057, respectively. The larger groups $\mathcal{G}_1, \mathcal{G}_4$ are referred to as *majority groups* and the smaller $\mathcal{G}_2, \mathcal{G}_3$ are referred to as minority groups. As a result of this heavy imbalance, the background becomes a *spurious feature*, i.e. it is a feature that is correlated with the target on the train data, but it is not predictive of the target on the minority groups. Throughout the paper we will discuss multiple examples of spurious correlations in both natural and synthetic datasets. In this paper, we study the effect of spurious correlations on the features learned by standard neural networks, and based on our findings propose a simple way of reducing the reliance on spurious features assuming access to a small set of data where the groups are equally represented.

3 Related Work

Feature learning in the presence of spurious correlations. The poor performance of neural networks on datasets with spurious correlations inspired research in understanding when and how the spurious features are learned. Geirhos et al. (2020) provide a detailed survey of the results in this area. Several works explore the behavior of maximum-margin classifiers, SGD training dynamics and inductive biases of neural network models in the presence of spurious features (Nagarajan et al., 2020; Pezeshki et al., 2021; Rahaman et al., 2019). Shah et al. (2020) show empirically that in certain scenarios neural networks can suffer from *extreme simplicity bias* and rely on simple spurious features, while ignoring the core features; in Section 4.2 we revisit these problems and provide further discussion. Hermann & Lampinen (2020) and Jacobsen et al. (2018) also show synthetic and natural examples, where neural networks ignore relevant features, and Scimeca et al. (2021) explore which types of shortcuts are more likely to be learned. Kolesnikov & Lampert (2016) on the other hand show that on realistic datasets core and spurious features can often be distinguished from the latent representations learned by a neural network in the context of object localization. In an independent and concurrent work, Rosenfeld et al. (2022) show that standard ERM learns high quality representations in the context of domain generalization, and by training the last layer on the target domain it is possible to achieve strong results. Kang et al. (2019) propose to use classifier re-training among other methods in the context of long-tail classification. The observations in our work are complimentary, as they focus on different settings.

Group robustness. The methods achieving the best worst-group performance typically build on the distributionally robust optimization (DRO) framework, where the worst-case loss is minimized instead of the average loss (Ben-Tal et al., 2013; Hu et al., 2018; Sagawa et al., 2019; Oren et al., 2019; Zhang et al., 2020). Notably, Group DRO (Sagawa et al., 2019), which optimizes a soft version of the worst-group loss holds state-of-the-art results on multiple benchmarks with spurious correlations. Several methods have been proposed for the scenario where group labels are not known, and need to be inferred from the data; these methods typically train a pair of networks, where the first model is used to identify the challenging minority examples and define a weighted loss for the second model (Liu et al., 2021; Nam et al., 2020; Yaghoobzadeh et al., 2019; Utama et al., 2020; Creager et al., 2021; Dagaev et al., 2021; Zhang et al., 2022). Other works proposed semi-supervised methods for the scenario where the group labels are provided for a small fraction of the train datapoints (Sohoni et al., 2021; Nam et al., 2022). Idrissi et al. (2021) recently showed that with careful tuning simple approaches such as data subsampling and reweighting can provide competitive performance. We note that all of the methods described above use a validation set with a high representation of minority groups to tune the hyper-parameters and optimize worst-group performance.

In a closely related work, Menon et al. (2020) considered classifier retraining and threshold correction on a subset of the training data for correcting the subgroup bias. In our work, we focus on classifier retraining and show that re-using train data for last layer retraining as done in Menon et al. (2020) is suboptimal, while retraining the last layer on held-out data achieves significantly better performance across various spurious correlations benchmarks (see Section 6). Moreover, we make multiple contributions beyond the scope of Menon et al. (2020), for example: we analyze feature learning in the extreme simplicity bias scenarios (Section 4), show strong performance on natural language processing datasets with spurious correlations (Section 6) and demonstrate how last layer retraining can be used to correct shape and texture bias in large-scale models on ImageNet (Section 7).

Due to the page limit, we provide further discussion of prior work in spurious correlations, transfer learning and other related areas in Appendix A.

4 Understanding Representation Learning with Spurious Correlations

In this section we investigate the solutions learned by standard ERM classifiers on datasets with spurious correlations. We show that while these classifiers underperform on the minority groups, they still learn the core features that can be used to make correct predictions on the minority groups.

4.1 Feature learning on Waterbirds data

We first consider the Waterbirds dataset (Sagawa et al., 2019) (see Section 2) which is generated synthetically by combining images of birds from the CUB dataset (Wah et al., 2011) and backgrounds from the Places dataset (Zhou et al., 2017) (see Sagawa et al. (2019) for a detailed description of the data generation process). For the experiments in this section, we generate several variations of the Waterbirds data following the procedure analogous to Sagawa et al. (2019). The *Original* dataset is analogous to the standard Waterbirds data, but we vary the degree of spurious correlation between the background and the target: 50% (*Balanced* dataset), 95% (as in Sagawa et al. (2019)) and 100% (no minority group examples in the train dataset). The *FG-Only* dataset contains images of the birds on uniform grey background instead of the Places background, removing the spurious feature. We show examples of datapoints from each variation of the dataset in Appendix Figure 4. In Appendix B.1, we provide the full details for the experiment in this section, and additionally consider the reverse Waterbirds problem, where instead of predicting the bird type, the task is to predict the background type, with similar results.

Train Data	**Test Data (Worst Acc)**	
(Spurious Corr.)	Original	FG-Only
Balanced (50%)	91.9%	94.7%
Original (95%)	73.8%	93.7%
Original (100%)	38.4%	94%
FG-Only (-)	75.2%	95.5%

Table 1: ERM classifiers trained on Waterbirds with Original and FG-Only images achieve similar FG-Only accuracy.

We train a ResNet-50 model with ERM on each of the variations of the data and report the results in Table 1. Following prior work (e.g., Sagawa et al., 2019; Liu et al., 2021; Idrissi et al., 2021), we initialize the model with weights pretrained on ImageNet. For the models trained on the Original data, there is a large difference between the mean and worst group accuracy on the Original test

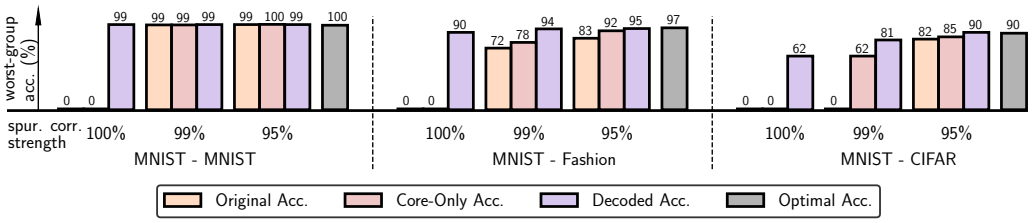

Figure 2: **Feature learning and simplicity bias.** ResNet-20 ERM classifiers trained on Dominoes data with varying levels of spurious correlation between core and spurious features. We show worst-group test accuracy for: Original data, data with only core features present (Core-Only), and accuracy of decoding the core feature from the latent representations of the Original data with logistic regression. We additionally report optimal accuracy: accuracy of a model trained and evaluated on the Core-Only data. Even in cases when the model achieves 0% accuracy on the Original data, the core features can still be decoded from latent representations.

data: the model heavily relies on the background information in its predictions, so the performance on minority groups is poor. The model trained without minority groups is especially affected, only achieving 38.4% worst group accuracy. However, surprisingly, we find that all the models trained on the Original data can make much better predictions on the FG-Only test data: if we remove the spurious feature (background) from the inputs at test time, the models make predictions based on the core feature (bird), and achieve worst-group[1] accuracy close to 94%, which is only slightly lower than the accuracy of a model trained directly on the FG-Only data and comparable to the accuracy of a model that was trained on balanced train data.

In Appendix B.4, we try to understand how the features from the foreground and the background interact with each other in a Waterbirds-trained neural network. We find a phenomenon that we call *logit additivity*: the class logits on a Waterbirds image are well approximated as the sum of the logits for the corresponding background image and the logits for the corresponding foreground image.

In summary, we conclude that while the models trained on the Original data make use of background information to make predictions, they still learn the features relevant to classifying the birds *almost as well as the models trained on the data without spurious correlations*. We will see that we can retrain the last layer of the Original-trained models and dramatically improve the worst-group performance on the Original data, by emphasizing the features relevant to the bird instead of the background.

4.2 Simplicity bias

Shah et al. (2020) showed that neural networks can suffer from *extreme simplicity bias*, a tendency to completely rely on the simple features, while ignoring similarly predictive (or even more predictive) complex features. In this section, we explore whether the neural networks can still learn the core features in the extreme simplicity bias scenarios, where the spurious features are simple and highly correlated with the target. Following Shah et al. (2020) and Pagliardini et al. (2022), we consider *Dominoes* binary classification datasets, where the top half of the image shows MNIST digits (LeCun et al., 1998) from classes $\{0, 1\}$, and the bottom half shows MNIST images from classes {7, 9} (*MNIST-MNIST*), Fashion-MNIST (Xiao et al., 2017) images from classes {coat, dress} (*MNIST-Fashion*) or CIFAR-10 (Krizhevsky et al., 2009) images from classes {car, truck} (*MNIST-CIFAR*). In all Dominoes datasets, the top half of the image (MNIST $0 - 1$ images) presents a linearly separable feature; the bottom half of the image presents a harder to learn feature. See Appendix B.2 for more details about the experimental set-up and datasets, and Appendix Figure 4 for image examples.

We use the simple feature (top half of the images) as a spurious feature and the complex feature (bottom half) as the core feature; we generate datasets with $100\%, 99\%$ and 95% correlations between the spurious feature and the target in train data, while the core feature is perfectly aligned with the target. We then define 4 groups $\mathcal{G}_i$ based on the values of the spurious and core features, where the minority groups correspond to images with top and bottom halves that do not match. The groups on validation and test are balanced.

[1]On the FG-Only data the groups only differ by the bird type, as we remove the background. The difference between mean and worst-group accuracy is because the target classes are not balanced in the training data.

We train a ResNet-20 model on each variation of the dataset. In Figure 2 we report the worst group performance for each of the datasets and each spurious correlation strength. In addition to the worst-group accuracy on the Original test data, we report the *Core-Only* worst-group accuracy, where we evaluate the model on datapoints with the spurious top half of the image replaced with a black image. Similarly to Shah et al. (2020) and Pagliardini et al. (2022), we observe that when the spurious features are perfectly correlated with the target on Dominoes datasets, the model relies just on the simple spurious feature to make predictions and achieves 0% worst-group accuracy. However, with 99% and 95% spurious correlation levels on train, we observe that models learned the core features well, as indicated both by their performance on the Original test data and especially increased performance on Core-Only test data where spurious features are absent. For reference, on each dataset we also report the *Optimal accuracy*, which is the accuracy of a model trained and evaluated on the Core-Only data. The optimal accuracy provides an upper bound on the accuracy that we can expect on each of the datasets.

Decoding feature representations. The performance on the Original and even Core-Only data might not be fully representative of whether or not the network learned a high-quality representation of the core features. Indeed, even if we remove the MNIST digit from the top half of the image, the network can still primarily rely on the (empty) top half in its predictions: an empty image may be more likely to come from class 1, which typically has fewer white pixels than class 0. To see how much information about the core feature is contained in the latent representation, we evaluate the *decoded* accuracy: for each problem we train a logistic regression classifier on the features extracted by the final convolutional layer of the network. We use a group-balanced validation set to train the logistic regression model, and then report the worst-group accuracy on a test set. In Figure 2, we observe that for MNIST-MNIST and MNIST-FashionMNIST even when the spurious correlation is 100%, reweighting the features leads to high worst group test accuracy. Moreover, on all Dominoes datasets for 99% and 95% spurious correlations level the core features can be decoded with high accuracy and almost match the optimal accuracy. This decoding serves as a basis of our DFR method, which we describe in detail in Section 5. In Appendix B.2 we report an additional baseline and verify that the model indeed learns a non-trivial representation of the core feature.

Relation to prior work. With the same Dominoes datasets that we consider in this section, Shah et al. (2020) showed that neural networks tend to rely entirely on the simple features. However, they only considered the 100% spurious correlation strength and accuracy on the Original test data. Our results do not contradict their findings but provide new insights: even in these most challenging cases, the networks still represent information about the complex core feature. Moreover, this information can be decoded to achieve high accuracy on the mixed group examples. Hermann & Lampinen (2020) considered a different set of synthetic datasets, showing that in some cases neural networks fail to represent information about some of the predictive features. In particular, they also considered decoding the information about these features from the latent representations and different spurious correlation strengths. Our results add to their observations and show that while it is possible to construct examples where predictive features are suppressed, in many challenging practical scenarios, neural networks learn a high quality representation of the core features relevant to the problem even if they rely on the spurious features.

ColorMNIST. In Appendix B.3 we additionally show results on ColorMNIST dataset with varied spurious correlations strength in train data: decoding core features from the trained representations on this problem also achieves results close to optimal accuracy and demonstrates that the core features are learned even in the cases when the model initially achieved 0% worst-group accuracy.

In summary, we find that, surprisingly, if (1) the strength of the spurious correlation is lower than 100% or (2) the difference in complexity between the core and spurious features is not as stark as on MNIST-CIFAR, *the core feature can be decoded from the learned embeddings with high accuracy*.

5 Deep Feature Reweighting

In Section 4 we have seen that neural networks trained with standard ERM learn multiple features relevant to the predictive task, such as features of both the background and the object represented in the image. Inspired by these observations, we propose *Deep Feature Reweighting (DFR)*, a simple and practical method for improving robustness to spurious correlations and distribution shift.

Let us assume that we have access to a dataset $\mathcal{D} = \{x_i, y_i\}$ which can exhibit spurious correlations. Furthermore, we assume that we have access to a (typically much smaller) dataset $\hat{\mathcal{D}}$, where the groups are represented equally. $\hat{\mathcal{D}}$ can be a subset of the train dataset $\mathcal{D}$, or a separate set of datapoints. We will refer to $\hat{\mathcal{D}}$ as *reweighting dataset*. We start by training a neural network on all of the available data $\mathcal{D}$ with standard ERM without any group or class reweighting. For this stage we do not need any information beyond the training data and labels. Here, we assume that the network consists of a feature extractor (such as a a sequence of convolutional or transformer layers), followed by a fully-connected classification layer mapping the features to class logits. In the second stage of the procedure, we simply discard the classification head and train a new classification head from scratch on the available balanced data $\hat{\mathcal{D}}$. We use the new classification head to make predictions on the test data. We illustrate DFR in Figure 1. **Notation:** we will use notation DFR$^{\hat{\mathcal{D}}}_{\mathcal{D}}$, where $\mathcal{D}$ is the dataset used to train the base feature extractor model and $\hat{\mathcal{D}}$ – to train the last linear layer.

6 Feature Reweighting Improves Robustness

In this section, we evaluate DFR on benchmark problems with spurious correlations.

Data. See Section 2 for a description of the *Waterbirds* data. On *CelebA* hair color prediction(Liu et al., 2015), the groups are non-blond females ($\mathcal{G}_1$), blond females ($\mathcal{G}_2$), non-blond males ($\mathcal{G}_3$) and blond males ($\mathcal{G}_4$) with proportions $44\%, 14\%, 41\%$, and 1% of the data, respectively; the group $\mathcal{G}_4$ is the minority group, and the gender serves as a spurious feature. On *MultiNLI*, the goal is to classify the relation between a pair of sentences (premise and hypothesis) as contradiction, entailment or neutral; the presence of negation words ("no", "never", ...) is correlated with the contradiction class, and serves as a spurious feature. Finally, we consider the *CivilComments* (Borkan et al., 2019) dataset implemented in the WILDS benchmark (Koh et al., 2021; Sagawa et al., 2021), where the goal is to classify comments as toxic or neutral. Each comment is labeled with 8 attributes s_i (male, female, LGBT, black, white, Christian, Muslim, other religion) based on whether or not the corresponding characteristic is mentioned in the comment. For evaluation, we follow the standard WILDS protocol and report the worst accuracy across the 16 overlapping groups corresponding to pairs (y, s_i) for each of the attributes s_i. See Figures 6, 7 for a visual description of all four datasets.

Baselines. We consider 6 baseline methods that work under different assumptions on the information available at the training time. *Empirical Risk Minimization* (*ERM*) represents conventional training without any procedures for improving worst-group accuracies. *Just Train Twice* (*JTT*) (Liu et al., 2021) is a method that detects the minority group examples on train data, only using group labels on the validation set to tune hyper-parameters. *Correct-n-Contrast* (*CnC*) (Zhang et al., 2022) detects the minority group examples similarly to JTT, and uses a contrastive objective to learn representations robust to spurious correlations. *Group DRO* (Sagawa et al., 2019) is a state-of-the-art method, which uses group information on train and adaptively upweights worst-group examples during training. *SUBG* is ERM applied to a random subset of the data where the groups are equally represented, which was recently shown to be a surprisingly strong baseline (Idrissi et al., 2021). Finally, *Spread Spurious Attribute* (*SSA*) (Nam et al., 2022) attempts to fully exploit the group-labeled validation data with a semi-supervised approach that propagates the group labels to the the training data. We discuss the assumptions on the data for each of these baselines in Appendix C.1.

DFR versions. We consider two variations of DFR$^{\hat{\mathcal{D}}}_{\mathcal{D}}$, which differ by the way we construct the balanced set $\hat{\mathcal{D}}$. In *DFR*$^{Tr}_{Tr}$, we use a random group-balanced[2] subset of the train data as $\hat{\mathcal{D}}$, i.e. we keep all of the data from the smallest group, and subsample the data from the other groups to the same size. In *DFR*$^{Val}_{Tr}$, we use a balanced subset of the validation data available for each of the problems. We use the standard training dataset (with group imbalance) as $\mathcal{D}$. In order to make use of more of the available data, we train logistic regression 10 times using different random balanced subsets of the data, and average the weights of the learned models. Full details are available in Appendix C.

Hyper-parameters. Following prior work (e.g. Liu et al., 2021), we use a ResNet-50 model (He et al., 2016) pretrained on ImageNet for Waterbirds and CelebA and a BERT model (Devlin et al., 2018) pre-trained on Book Corpus and English Wikipedia data for MultiNLI and CivilComments. For all DFR variations, the size of the reweighting set $\hat{\mathcal{D}}$ is small relative to the number of features

[2]On CivilComments the groups overlap, so for each datapoint we use the smallest group that contains it when constructing the group-balanced reweighting dataset.

Method	Group Info	Waterbirds		CelebA		MultiNLI		CivilComments	
	Train / Val	Worst(%)	Mean(%)	Worst(%)	Mean(%)	Worst(%)	Mean(%)	Worst(%)	Mean(%)
JTT	✗ / ✓	86.7	93.3	81.1	88.0	72.6	78.6	69.3	91.1
CnC	✗ / ✓	$88.5_{\pm 0.3}$	$90.9_{\pm 0.1}$	$88.8_{\pm 0.9}$	$89.9_{\pm 0.5}$	-	-	$68.9_{\pm 2.1}$	$81.7_{\pm 0.5}$
SUBG	✓ / ✓	$89.1_{\pm 1.1}$	-	$85.6_{\pm 2.3}$	-	$68.9_{\pm 0.8}$	-	-	-
SSA	✗ / ✓✓	$89.0_{\pm 0.6}$	$92.2_{\pm 0.9}$	$\mathbf{89.8}_{\pm 1.3}$	$92.8_{\pm 0.1}$	$76.6_{\pm 0.7}$	$79.9_{\pm 0.87}$	$\mathbf{69.9}_{\pm 2}$	$88.2_{\pm 2.}$
Group DRO	✓ / ✓	91.4	93.5	88.9	92.9	**77.7**	81.4	**69.9**	88.9
Base (ERM)	✗ / ✗	$74.9_{\pm 2.4}$	$98.1_{\pm 0.1}$	$46.9_{\pm 2.8}$	$95.3_{\pm 0}$	$65.9_{\pm 0.3}$	$82.8_{\pm 0.1}$	$55.6_{\pm 0.6}$	$92.1_{\pm 0.1}$
$\text{DFR}^{\text{Tr}}_{\text{Tr}}$	✓ / ✓	$90.2_{\pm 0.8}$	$97.0_{\pm 0.3}$	$80.7_{\pm 2.4}$	$90.6_{\pm 0.7}$	$71.5_{\pm 0.6}$	$82.5_{\pm 0.2}$	$58.0_{\pm 1.3}$	$92.0_{\pm 0.1}$
$\text{DFR}^{\text{Val}}_{\text{Tr}}$	✗ / ✓✓	$\mathbf{92.9}_{\pm 0.2}$	$94.2_{\pm 0.4}$	$88.3_{\pm 1.1}$	$91.3_{\pm 0.3}$	$74.7_{\pm 0.7}$	$82.1_{\pm 0.2}$	$\mathbf{70.1}_{\pm 0.8}$	$87.2_{\pm 0.3}$

Table 2: **Spurious correlation benchmark results.** Worst-group and mean test accuracy of DFR variations and baselines on benchmark datasets. For mean accuracy, we follow Sagawa et al. (2019) and weight the group accuracies according to their prevalence in the training data. The Group Info column shows whether group labels are available to the methods on train and validation datasets. $\text{DFR}^{\text{Val}}_{\text{Tr}}$ uses the validation data to train the model parameters (last layer) in addition to hyper-parameter tuning, indicated with ✓✓; SSA also uses the validation set to train the model. For DFR we report the mean$\pm$std over 5 independent runs. DFR is competitive with state-of-the-art.

produced by the feature extractor. For this reason, we use ℓ_1-regularizaion to allow the model to learn sparse solutions and drop irrelevant features. For $\text{DFR}^{\text{Val}}_{\text{Tr}}$ *we only tune a single hyper-parameter* — the strength of the regularization term. For $\text{DFR}^{\text{Tr}}_{\text{Tr}}$ we additionally tune separate weights for the classes, because unlike $\text{DFR}^{\text{Val}}_{\text{Tr}}$, in $\text{DFR}^{\text{Tr}}_{\text{Tr}}$ the feature extractor and the last layer are trained on the same minority data, and logistic regression with equal class weights tends to underperform on the minority groups. We tune all the hyper-parameters on the validation data provided with each of the datasets. We note that the prior work methods including Group DRO, JTT, CnC, SUBG, SSA and others extensively tune hyper-parameters on the validation data. For $\text{DFR}^{\text{Val}}_{\text{Tr}}$ we split the validation in half, and use one half to tune the regularization strength parameter; then, we retrain the logistic regression with the optimal regularization on the full validation set.

Results. We report the results for DFR and the baselines in Table 2. $\text{DFR}^{\text{Val}}_{\text{Tr}}$ is competitive with the state-of-the-art Group DRO across the board, achieving the best results among all methods on Waterbirds and CivilComments. Moreover, $\text{DFR}^{\text{Val}}_{\text{Tr}}$ achieves similar performance to SSA, a method designed to make optimal use of the group information on the validation data ($\text{DFR}^{\text{Val}}_{\text{Tr}}$ is slightly better on Waterbirds and CivilComments while SSA is better on CelebA and MultiNLI). Both methods use the same exact setting and group information to train and tune the model. $\text{DFR}^{\text{Tr}}_{\text{Tr}}$ also significantly improves performance compared to the base model accross the board, but underperforms compared to $\text{DFR}^{\text{Val}}_{\text{Tr}}$: it is crucial to retrain the last layer on new data that was not used to train the feature extractor. We explore this effect further in Appendix C.3.

To sum up, $\text{DFR}^{\text{Val}}_{\text{Tr}}$ matches the performance of the best available methods, while only using the group labels on a small validation set. This state-of-the-art performance is achieved by simply reweighting the features learned by standard ERM, with no need for advanced regularization techniques.

7 Natural Spurious Correlations on ImageNet

In the previous section we focused on benchmark problems constructed to highlight the effect of spurious features. Computer vision classifiers are known to learn undesirable patterns and rely on spurious features in real-world problems (see e.g. Rosenfeld et al., 2018; Singla & Feizi, 2021; Geirhos et al., 2020). In this section we explore two prominent shortcomings of ImageNet classifiers: background reliance (Xiao et al., 2020) and texture bias (Geirhos et al., 2018).

7.1 Background Reliance

Prior work has demonstrated that computer vision models such as ImageNet classifiers can rely on image background to make their predictions (Zhang et al., 2007; Ribeiro et al., 2016; Shetty et al., 2019; Xiao et al., 2020; Singla & Feizi, 2021). Here, we show that it is possible to reduce the background reliance of ImageNet-trained models by simply retraining their last layer with DFR.

Xiao et al. (2020) proposed several datasets in the *Backgrounds Challenge* to study the effect of the backgrounds on predictions of ImageNet models. The datasets in the Backgrounds Challenge are based on the ImageNet-9 dataset, a subset of ImageNet structured into 9 coarse-grain classes

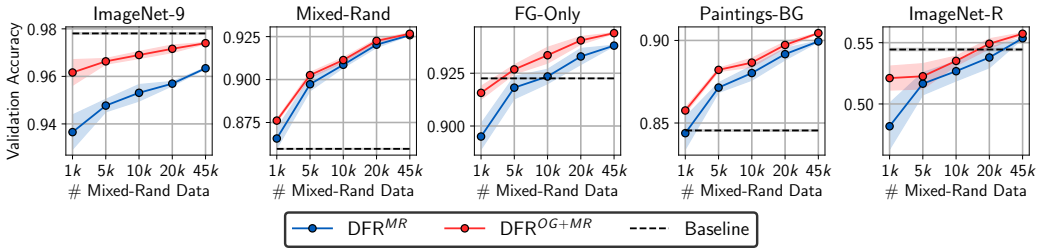

Figure 3: **Background reliance.** Accuracy of DFR^{MR}and DFR$^{\text{OG+MR}}$ on different ImageNet-9 validation splits with an ImageNet-trained ResNet-50 feature extractor. DFR reduces background reliance with a minimal drop in performance on the Original data.

(see Xiao et al. (2020) for details). ImageNet-9 contains $45k$ training images and 4050 validation images. We consider three datasets from the Backgrounds Challenge: (1) *Original* contains the original images; (2) *Mixed-Rand* contains images with random combinations of backgrounds and foregrounds (objects); (3) *FG-Only* contains images showing just the object with a black background. We additionally consider *Paintings-BG* using paintings from Kaggle's `painter-by-numbers` dataset (`https://www.kaggle.com/c/painter-by-numbers/`) as background for the ImageNet-9 validation data. Finally, we consider the ImageNet-R dataset (Hendrycks et al., 2021) restricted to the ImageNet-9 classes. See Appendix D for details and Figure 11 for example images.

We use an ImageNet-trained ResNet-50 as a feature extractor and train DFR with different reweighting datasets. As a *Baseline*, we train DFR on the Original $45k$ training datapoints (we cannot use the ImageNet-trained ResNet-50 last layer, as ImageNet-9 has a different set of classes). We train *DFR^{MR}* and *DFR^{OG+MR}* on Mixed-Rand training data and a combination of Mixed-Rand and Original training data respectively. In Figure 3, we report the predictive accuracy of these methods on different validation datasets as a function of the number of Mixed-Rand data observed. We select the observed subset of the data randomly; for DFR$^{\text{OG+MR}}$, in each case we use the same amount of Mixed-Rand and Original training datapoints. We repeat this experiment with a VIT-B-16 model (Dosovitskiy et al., 2020) pretrained on ImageNet-21k and report the results in the Appendix Figure 9.

First, we notice that the baseline model provides significantly better performance on FG-Only (92%) than on the Mixed-Rand (86%) validation set, suggesting that the feature extractor learned the features needed to classify the foreground, as well as the background features. With access to Mixed-Rand data, we can reweight the foreground and background features with DFR and significantly improve the performance on mixed-rand, FG-Only and Paintings-BG datasets. At the same time, DFR$^{\text{OG+MR}}$ is able to mostly maintain the performance on the Original ImageNet-9 data; the small drop in performance is because the background is relevant to predicting the class on this validation set. Finally, on ImageNet-R, DFR provides a small improvement when we use all of $45k$ datapoints; the covariate shift in ImageNet-R is not primarily background-based, so reducing background reliance does not provide a big improvement. We provide additional results in See Appendix D.

7.2 Texture-vs-shape bias

Geirhos et al. (2018) showed that on images with conflicting texture and shape, ImageNet-trained CNNs tend to make predictions based on the texture, while humans usually predict based on the shape of the object. The authors designed the *GST* dataset with conflicting cues, and proposed the term *texture bias* to refer to the fraction of datapoints on which a model (or a human) makes predictions based on texture; conversely, *shape bias* is the fraction of the datapoints on which prediction is made based on the shape of the object. Geirhos et al. (2018) showed that it is possible to increase the shape bias of CNNs by training on Stylized ImageNet (*SIN*), a dataset obtained from ImageNet by removing the texture information via style transfer (see Appendix Figure 11 for example images). Using SIN in combination with ImageNet (*SIN+IN*), they also obtained improved robustness to corruptions. Finally, they proposed the *Shape-RN-50* model, a ResNet-50 (RN-50) trained on SIN+IN and finetuned on IN, which outperforms the ImageNet-trained ResNet-50 on in-distribution data and out-of-distribution robustness.

Method	Training Data	Shape bias (%)	Top-1 Acc (%) / Top-5 Acc (%)		
			ImageNet	ImageNet-R	ImageNet-C
RN-50	IN	21.4	76.0/92.9	23.8/36.6	39.8/60.7
	SIN	**81.4**	60.3/82.7	26.9/42.1	38.1/59.7
	IN+SIN	34.7	74.6/92.1	**27.6/42.5**	**45.7/67.4**
Shape-RN-50	IN+SIN	20.5	**76.8/93.3**	25.6/39.8	42.3/63.3
DFR	SIN	<u>34.0</u>	65.1/85.7	24.6/39.4	36.7/56.7
	IN+SIN	30.6	<u>74.5/91.8</u>	<u>**27.2/42.4**</u>	<u>40.7/61.3</u>

Table 3: **Shape bias.** Shape bias and accuracy on ImageNet validation set variations for ResNet-50 trained on different datasets and DFR with an ImageNet-trained ResNet-50 as a feature extractor. For each metric, we show the best result in bold and underline the best result among DFR methods. By retraining just the last layer with DFR, we can significantly increase the shape bias compared to the base model ($21.4\% \rightarrow 34\%$ for DFR(SIN)) and improve performance on ImageNet-R/C.

Here, we explore whether it is possible to change the shape bias of ImageNet-trained models by simply retraining the last layer with DFR. Intuitively, we expect that the standard ImageNet-trained model already learns *both* the shape and texture features. Indeed, Hermann et al. (2020) showed that shape information is partially decodable from the features of ImageNet models on the GST dataset. Here, instead of targeting GST, we apply DFR to the large-scale SIN dataset, and explore both the shape bias and the predictive performance of the resulting models. In Table 3, we report the shape bias, as well as predictive accuracy of ResNet-50 models trained on ImageNet (*IN*), SIN, IN+SIN and the Shape-RN-50 model, and the DFR models trained on SIN and IN+SIN. The DFR models use an IN-trained ResNet-50 model as a feature extractor. See Appendix E for details.

First, we observe that while the SIN-trained RN-50 achieves a shape-bias of 81.4%, as reported by Geirhos et al. (2018), the models trained on combinations of IN and SIN are still biased towards texture. Curiously, the Shape-RN-50 model proposed by Geirhos et al. (2018) has almost identical shape bias to a standard IN-trained RN-50! At the same time, Shape-RN-50 outperforms IN-trained RN-50 on all the datasets that we consider, and Geirhos et al. (2018) showed that Shape-RN-50 significantly outperforms IN-trained RN-50 in transfer learning to a segmentation problem, suggesting that it learned better shape-based features. The fact that the shape bias of this model is lower than that of an IN-trained RN-50, suggests that the shape bias is largely affected by the last linear layer of the model: even if the model extracted high-quality features capturing the shape information, the last layer can still assign a higher weight to the texture information.

Next, DFR can significantly increase the shape bias of an IN-trained model. $\text{DFR}_{\text{IN}}^{\text{SIN}}$ achieves a comparable shape-bias to that of a model trained from scratch on a combination of IN and SIN datasets. Finally, $\text{DFR}_{\text{IN}}^{\text{IN+SIN}}$ improves the performance on both ImageNet-R and ImageNet-C (Hendrycks & Dietterich, 2019) datasets compared to the base RN-50 model. In the Appendix Table 10 we show similar results for a VIT-B-16 model pretrained on ImageNet-21k and finetuned on ImageNet; there, $\text{DFR}_{\text{IN}}^{\text{IN+SIN}}$ can also improve the shape-bias and performance on ImageNet-C, but does not help on ImageNet-R. To sum up, by reweighting the features learned by an ImageNet-trained model, we can significantly increase its shape bias and improve robustness to certain corruptions. However, to achieve the highest possible shape bias, it is still preferable to re-train the model from scratch, as RN-50(SIN) achieves a much higher shape bias compared to all other methods.

8 Discussion

We have shown that neural networks simultaneously learn multiple different features, including relevant semantic structure, even in the presence spurious correlations. By retraining the last layer of the network with DFR, we can significantly reduce the impact of spurious features and improve worst-group-performance of the models. In particular, DFR achieves state-of-the-art performance on spurious correlation benchmarks, and can reduce the reliance of ImageNet trained models on background and texture information. DFR is extremely simple, cheap and effective: it only has one hyper-parameter, and we can run it on ImageNet-scale data in a matter of minutes. We hope that our results will be useful to practitioners and will inspire further research in feature learning in the presence of spurious correlations. We provide further discussion in Appendix F.

REFERENCES

Samira Abnar, Mostafa Dehghani, Behnam Neyshabur, and Hanie Sedghi. Exploring the limits of large scale pre-training. *arXiv preprint arXiv:2110.02095*, 2021.

Alekh Agarwal, Alina Beygelzimer, Miroslav Dudík, John Langford, and Hanna Wallach. A reductions approach to fair classification. In *International Conference on Machine Learning*, pp. 60–69. PMLR, 2018.

Michael A Alcorn, Qi Li, Zhitao Gong, Chengfei Wang, Long Mai, Wei-Shinn Ku, and Anh Nguyen. Strike (with) a pose: Neural networks are easily fooled by strange poses of familiar objects. In *Proceedings of the IEEE/CVF Conference on Computer Vision and Pattern Recognition*, pp. 4845–4854, 2019.

Martin Arjovsky, Léon Bottou, Ishaan Gulrajani, and David Lopez-Paz. Invariant risk minimization. *arXiv preprint arXiv:1907.02893*, 2019.

Benjamin Aubin, Agnieszka Słowik, Martin Arjovsky, Leon Bottou, and David Lopez-Paz. Linear unit-tests for invariance discovery. *arXiv preprint arXiv:2102.10867*, 2021.

Hyojin Bahng, Sanghyuk Chun, Sangdoo Yun, Jaegul Choo, and Seong Joon Oh. Learning de-biased representations with biased representations. In *International Conference on Machine Learning*, pp. 528–539. PMLR, 2020.

Sara Beery, Grant Van Horn, and Pietro Perona. Recognition in terra incognita. In *Proceedings of the European conference on computer vision (ECCV)*, pp. 456–473, 2018.

Aharon Ben-Tal, Dick Den Hertog, Anja De Waegenaere, Bertrand Melenberg, and Gijs Rennen. Robust solutions of optimization problems affected by uncertain probabilities. *Management Science*, 59(2):341–357, 2013.

Gilles Blanchard, Gyemin Lee, and Clayton Scott. Generalizing from several related classification tasks to a new unlabeled sample. *Advances in neural information processing systems*, 24, 2011.

Rishi Bommasani, Drew A Hudson, Ehsan Adeli, Russ Altman, Simran Arora, Sydney von Arx, Michael S Bernstein, Jeannette Bohg, Antoine Bosselut, Emma Brunskill, et al. On the opportunities and risks of foundation models. *arXiv preprint arXiv:2108.07258*, 2021.

Daniel Borkan, Lucas Dixon, Jeffrey Sorensen, Nithum Thain, and Lucy Vasserman. Nuanced metrics for measuring unintended bias with real data for text classification. In *Companion proceedings of the 2019 world wide web conference*, pp. 491–500, 2019.

Wieland Brendel and Matthias Bethge. Approximating cnns with bag-of-local-features models works surprisingly well on imagenet. *arXiv preprint arXiv:1904.00760*, 2019.

Remi Cadene, Corentin Dancette, Matthieu Cord, Devi Parikh, et al. Rubi: Reducing unimodal biases for visual question answering. *Advances in neural information processing systems*, 32, 2019.

Kaidi Cao, Colin Wei, Adrien Gaidon, Nikos Arechiga, and Tengyu Ma. Learning imbalanced datasets with label-distribution-aware margin loss. *Advances in neural information processing systems*, 32, 2019.

Kaidi Cao, Yining Chen, Junwei Lu, Nikos Arechiga, Adrien Gaidon, and Tengyu Ma. Heteroskedastic and imbalanced deep learning with adaptive regularization. *arXiv preprint arXiv:2006.15766*, 2020.

Ting Chen, Simon Kornblith, Mohammad Norouzi, and Geoffrey Hinton. A simple framework for contrastive learning of visual representations. In *International conference on machine learning*, pp. 1597–1607. PMLR, 2020.

Elliot Creager, Jörn-Henrik Jacobsen, and Richard Zemel. Environment inference for invariant learning. In *International Conference on Machine Learning*, pp. 2189–2200. PMLR, 2021.

Nikolay Dagaev, Brett D Roads, Xiaoliang Luo, Daniel N Barry, Kaustubh R Patil, and Bradley C Love. A too-good-to-be-true prior to reduce shortcut reliance. *arXiv preprint arXiv:2102.06406*, 2021.

Jacob Devlin, Ming-Wei Chang, Kenton Lee, and Kristina Toutanova. Bert: Pre-training of deep bidirectional transformers for language understanding. *arXiv preprint arXiv:1810.04805*, 2018.

Alexey Dosovitskiy, Lucas Beyer, Alexander Kolesnikov, Dirk Weissenborn, Xiaohua Zhai, Thomas Unterthiner, Mostafa Dehghani, Matthias Minderer, Georg Heigold, Sylvain Gelly, et al. An image is worth 16x16 words: Transformers for image recognition at scale. *arXiv preprint arXiv:2010.11929*, 2020.

Cynthia Dwork, Moritz Hardt, Toniann Pitassi, Omer Reingold, and Richard Zemel. Fairness through awareness. In *Proceedings of the 3rd innovations in theoretical computer science conference*, pp. 214–226, 2012.

Jacob Eisenstein. Informativeness and invariance: Two perspectives on spurious correlations in natural language. In *Proceedings of the 2022 Conference of the North American Chapter of the Association for Computational Linguistics: Human Language Technologies*, pp. 4326–4331, 2022.

Yaroslav Ganin and Victor Lempitsky. Unsupervised domain adaptation by backpropagation. In *International conference on machine learning*, pp. 1180–1189. PMLR, 2015.

Yaroslav Ganin, Evgeniya Ustinova, Hana Ajakan, Pascal Germain, Hugo Larochelle, François Laviolette, Mario Marchand, and Victor Lempitsky. Domain-adversarial training of neural networks. *The journal of machine learning research*, 17(1):2096–2030, 2016.

Robert Geirhos, Patricia Rubisch, Claudio Michaelis, Matthias Bethge, Felix A Wichmann, and Wieland Brendel. Imagenet-trained cnns are biased towards texture; increasing shape bias improves accuracy and robustness. *arXiv preprint arXiv:1811.12231*, 2018.

Robert Geirhos, Jörn-Henrik Jacobsen, Claudio Michaelis, Richard Zemel, Wieland Brendel, Matthias Bethge, and Felix A Wichmann. Shortcut learning in deep neural networks. *Nature Machine Intelligence*, 2(11):665–673, 2020.

Robert Geirhos, Kantharaju Narayanappa, Benjamin Mitzkus, Tizian Thieringer, Matthias Bethge, Felix A Wichmann, and Wieland Brendel. Partial success in closing the gap between human and machine vision. In *Advances in Neural Information Processing Systems 34*, 2021.

Jacob Gildenblat and contributors. Pytorch library for cam methods. `https://github.com/jacobgil/pytorch-grad-cam`, 2021.

Ross Girshick. Fast r-cnn. In *Proceedings of the IEEE international conference on computer vision*, pp. 1440–1448, 2015.

Ishaan Gulrajani and David Lopez-Paz. In search of lost domain generalization. *arXiv preprint arXiv:2007.01434*, 2020.

Moritz Hardt, Eric Price, and Nati Srebro. Equality of opportunity in supervised learning. *Advances in neural information processing systems*, 29, 2016.

Charles R. Harris, K. Jarrod Millman, Stéfan J. van der Walt, Ralf Gommers, Pauli Virtanen, David Cournapeau, Eric Wieser, Julian Taylor, Sebastian Berg, Nathaniel J. Smith, Robert Kern, Matti Picus, Stephan Hoyer, Marten H. van Kerkwijk, Matthew Brett, Allan Haldane, Jaime Fernández del Río, Mark Wiebe, Pearu Peterson, Pierre Gérard-Marchant, Kevin Sheppard, Tyler Reddy, Warren Weckesser, Hameer Abbasi, Christoph Gohlke, and Travis E. Oliphant. Array programming with NumPy. *Nature*, 585(7825):357–362, September 2020. doi: 10.1038/s41586-020-2649-2. URL `https://doi.org/10.1038/s41586-020-2649-2`.

Kaiming He, Xiangyu Zhang, Shaoqing Ren, and Jian Sun. Deep residual learning for image recognition. In *Proceedings of the IEEE conference on computer vision and pattern recognition*, pp. 770–778, 2016.

Kaiming He, Georgia Gkioxari, Piotr Dollár, and Ross Girshick. Mask r-cnn. In *Proceedings of the IEEE international conference on computer vision*, pp. 2961–2969, 2017.

Kaiming He, Xinlei Chen, Saining Xie, Yanghao Li, Piotr Dollár, and Ross Girshick. Masked autoencoders are scalable vision learners. *arXiv preprint arXiv:2111.06377*, 2021.

Dan Hendrycks and Thomas Dietterich. Benchmarking neural network robustness to common corruptions and perturbations. *arXiv preprint arXiv:1903.12261*, 2019.

Dan Hendrycks, Steven Basart, Norman Mu, Saurav Kadavath, Frank Wang, Evan Dorundo, Rahul Desai, Tyler Zhu, Samyak Parajuli, Mike Guo, Dawn Song, Jacob Steinhardt, and Justin Gilmer. The many faces of robustness: A critical analysis of out-of-distribution generalization. *ICCV*, 2021.

Katherine Hermann and Andrew Lampinen. What shapes feature representations? exploring datasets, architectures, and training. *Advances in Neural Information Processing Systems*, 33:9995–10006, 2020.

Katherine Hermann, Ting Chen, and Simon Kornblith. The origins and prevalence of texture bias in convolutional neural networks. *Advances in Neural Information Processing Systems*, 33: 19000–19015, 2020.

Weihua Hu, Gang Niu, Issei Sato, and Masashi Sugiyama. Does distributionally robust supervised learning give robust classifiers? In *International Conference on Machine Learning*, pp. 2029–2037. PMLR, 2018.

Minyoung Huh, Pulkit Agrawal, and Alexei A Efros. What makes imagenet good for transfer learning? *arXiv preprint arXiv:1608.08614*, 2016.

J. D. Hunter. Matplotlib: A 2d graphics environment. *Computing in Science & Engineering*, 9(3): 90–95, 2007. doi: 10.1109/MCSE.2007.55.

Badr Youbi Idrissi, Martin Arjovsky, Mohammad Pezeshki, and David Lopez-Paz. Simple data balancing achieves competitive worst-group-accuracy. *arXiv preprint arXiv:2110.14503*, 2021.

Md Amirul Islam, Matthew Kowal, Patrick Esser, Sen Jia, Bjorn Ommer, Konstantinos G Derpanis, and Neil Bruce. Shape or texture: Understanding discriminative features in cnns. *arXiv preprint arXiv:2101.11604*, 2021.

Jörn-Henrik Jacobsen, Jens Behrmann, Richard Zemel, and Matthias Bethge. Excessive invariance causes adversarial vulnerability. *arXiv preprint arXiv:1811.00401*, 2018.

Bingyi Kang, Saining Xie, Marcus Rohrbach, Zhicheng Yan, Albert Gordo, Jiashi Feng, and Yannis Kalantidis. Decoupling representation and classifier for long-tailed recognition. *arXiv preprint arXiv:1910.09217*, 2019.

Divyansh Kaushik, Eduard Hovy, and Zachary Lipton. Learning the difference that makes a difference with counterfactually-augmented data. In *International Conference on Learning Representations*, 2020. URL `https://openreview.net/forum?id=Sklgs0NFvr`.

Divyansh Kaushik, Amrith Setlur, Eduard Hovy, and Zachary C Lipton. Explaining the efficacy of counterfactually augmented data. *International Conference on Learning Representations (ICLR)*, 2021.

Fereshte Khani, Aditi Raghunathan, and Percy Liang. Maximum weighted loss discrepancy. *arXiv preprint arXiv:1906.03518*, 2019.

Byungju Kim, Hyunwoo Kim, Kyungsu Kim, Sungjin Kim, and Junmo Kim. Learning not to learn: Training deep neural networks with biased data. In *Proceedings of the IEEE/CVF Conference on Computer Vision and Pattern Recognition*, pp. 9012–9020, 2019.

Jon Kleinberg, Sendhil Mullainathan, and Manish Raghavan. Inherent trade-offs in the fair determination of risk scores. *arXiv preprint arXiv:1609.05807*, 2016.

Thomas Kluyver, Benjamin Ragan-Kelley, Fernando Pérez, Brian Granger, Matthias Bussonnier, Jonathan Frederic, Kyle Kelley, Jessica Hamrick, Jason Grout, Sylvain Corlay, Paul Ivanov, Damián Avila, Safia Abdalla, and Carol Willing. Jupyter notebooks – a publishing format for reproducible computational workflows. In F. Loizides and B. Schmidt (eds.), *Positioning and Power in Academic Publishing: Players, Agents and Agendas*, pp. 87 – 90. IOS Press, 2016.

Pang Wei Koh, Shiori Sagawa, Henrik Marklund, Sang Michael Xie, Marvin Zhang, Akshay Balsubramani, Weihua Hu, Michihiro Yasunaga, Richard Lanas Phillips, Irena Gao, et al. Wilds: A benchmark of in-the-wild distribution shifts. In *International Conference on Machine Learning*, pp. 5637–5664. PMLR, 2021.

Alexander Kolesnikov and Christoph H Lampert. Improving weakly-supervised object localization by micro-annotation. *arXiv preprint arXiv:1605.05538*, 2016.

Alexander Kolesnikov, Lucas Beyer, Xiaohua Zhai, Joan Puigcerver, Jessica Yung, Sylvain Gelly, and Neil Houlsby. Big transfer (bit): General visual representation learning. In *European conference on computer vision*, pp. 491–507. Springer, 2020.

Simon Kornblith, Jonathon Shlens, and Quoc V Le. Do better imagenet models transfer better? In *Proceedings of the IEEE/CVF conference on computer vision and pattern recognition*, pp. 2661–2671, 2019.

Alex Krizhevsky, Geoffrey Hinton, et al. Learning multiple layers of features from tiny images. 2009.

David Krueger, Ethan Caballero, Joern-Henrik Jacobsen, Amy Zhang, Jonathan Binas, Dinghuai Zhang, Remi Le Priol, and Aaron Courville. Out-of-distribution generalization via risk extrapolation (rex). In *International Conference on Machine Learning*, pp. 5815–5826. PMLR, 2021.

Ananya Kumar, Aditi Raghunathan, Robbie Jones, Tengyu Ma, and Percy Liang. Fine-tuning can distort pretrained features and underperform out-of-distribution. *arXiv preprint arXiv:2202.10054*, 2022.

Yann LeCun, Léon Bottou, Yoshua Bengio, and Patrick Haffner. Gradient-based learning applied to document recognition. *Proceedings of the IEEE*, 86(11):2278–2324, 1998.

Yoonho Lee, Huaxiu Yao, and Chelsea Finn. Diversify and disambiguate: Learning from underspecified data. *arXiv preprint arXiv:2202.03418*, 2022.

Ya Li, Xinmei Tian, Mingming Gong, Yajing Liu, Tongliang Liu, Kun Zhang, and Dacheng Tao. Deep domain generalization via conditional invariant adversarial networks. In *Proceedings of the European Conference on Computer Vision (ECCV)*, pp. 624–639, 2018a.

Yi Li and Nuno Vasconcelos. Repair: Removing representation bias by dataset resampling. In *Proceedings of the IEEE/CVF conference on computer vision and pattern recognition*, pp. 9572–9581, 2019.

Yingwei Li, Yi Li, and Nuno Vasconcelos. Resound: Towards action recognition without representation bias. In *Proceedings of the European Conference on Computer Vision (ECCV)*, pp. 513–528, 2018b.

Evan Z Liu, Behzad Haghgoo, Annie S Chen, Aditi Raghunathan, Pang Wei Koh, Shiori Sagawa, Percy Liang, and Chelsea Finn. Just train twice: Improving group robustness without training group information. In *International Conference on Machine Learning*, pp. 6781–6792. PMLR, 2021.

Ziwei Liu, Ping Luo, Xiaogang Wang, and Xiaoou Tang. Deep learning face attributes in the wild. In *Proceedings of the IEEE international conference on computer vision*, pp. 3730–3738, 2015.

Ilya Loshchilov and Frank Hutter. Decoupled weight decay regularization. *arXiv preprint arXiv:1711.05101*, 2017.

Charles Lovering, Rohan Jha, Tal Linzen, and Ellie Pavlick. Predicting inductive biases of pre-trained models. In *International Conference on Learning Representations*, 2020.

Wesley Maddox, Shuai Tang, Pablo Moreno, Andrew Gordon Wilson, and Andreas Damianou. Fast adaptation with linearized neural networks. In *International Conference on Artificial Intelligence and Statistics*, pp. 2737–2745. PMLR, 2021.

Dhruv Mahajan, Ross Girshick, Vignesh Ramanathan, Kaiming He, Manohar Paluri, Yixuan Li, Ashwin Bharambe, and Laurens Van Der Maaten. Exploring the limits of weakly supervised pretraining. In *Proceedings of the European conference on computer vision (ECCV)*, pp. 181–196, 2018.

Sébastien Marcel and Yann Rodriguez. Torchvision the machine-vision package of torch. In *Proceedings of the 18th ACM international conference on Multimedia*, pp. 1485–1488, 2010.

R Thomas McCoy, Ellie Pavlick, and Tal Linzen. Right for the wrong reasons: Diagnosing syntactic heuristics in natural language inference. *arXiv preprint arXiv:1902.01007*, 2019.

Wes McKinney. Data structures for statistical computing in python. In Stéfan van der Walt and Jarrod Millman (eds.), *Proceedings of the 9th Python in Science Conference*, pp. 51 – 56, 2010.

Aditya Krishna Menon, Ankit Singh Rawat, and Sanjiv Kumar. Overparameterisation and worst-case generalisation: friend or foe? In *International Conference on Learning Representations*, 2020.

Mazda Moayeri, Phillip Pope, Yogesh Balaji, and Soheil Feizi. A comprehensive study of image classification model sensitivity to foregrounds, backgrounds, and visual attributes. *arXiv preprint arXiv:2201.10766*, 2022.

Krikamol Muandet, David Balduzzi, and Bernhard Schölkopf. Domain generalization via invariant feature representation. In *International Conference on Machine Learning*, pp. 10–18. PMLR, 2013.

Vaishnavh Nagarajan, Anders Andreassen, and Behnam Neyshabur. Understanding the failure modes of out-of-distribution generalization. *arXiv preprint arXiv:2010.15775*, 2020.

Junhyun Nam, Hyuntak Cha, Sungsoo Ahn, Jaeho Lee, and Jinwoo Shin. Learning from failure: De-biasing classifier from biased classifier. *Advances in Neural Information Processing Systems*, 33:20673–20684, 2020.

Junhyun Nam, Jaehyung Kim, Jaeho Lee, and Jinwoo Shin. Spread spurious attribute: Improving worst-group accuracy with spurious attribute estimation. In *International Conference on Learning Representations*, 2022.

Behnam Neyshabur, Hanie Sedghi, and Chiyuan Zhang. What is being transferred in transfer learning? *Advances in neural information processing systems*, 33:512–523, 2020.

Yonatan Oren, Shiori Sagawa, Tatsunori B Hashimoto, and Percy Liang. Distributionally robust language modeling. *arXiv preprint arXiv:1909.02060*, 2019.

Matteo Pagliardini, Martin Jaggi, François Fleuret, and Sai Praneeth Karimireddy. Agree to disagree: Diversity through disagreement for better transferability. *arXiv preprint arXiv:2202.04414*, 2022.

Sinno Jialin Pan and Qiang Yang. A survey on transfer learning. *IEEE Transactions on knowledge and data engineering*, 22(10):1345–1359, 2009.

Adam Paszke, Sam Gross, Soumith Chintala, Gregory Chanan, Edward Yang, Zachary DeVito, Zeming Lin, Alban Desmaison, Luca Antiga, and Adam Lerer. Automatic differentiation in pytorch. 2017.

F. Pedregosa, G. Varoquaux, A. Gramfort, V. Michel, B. Thirion, O. Grisel, M. Blondel, P. Prettenhofer, R. Weiss, V. Dubourg, J. Vanderplas, A. Passos, D. Cournapeau, M. Brucher, M. Perrot, and E. Duchesnay. Scikit-learn: Machine learning in Python. *Journal of Machine Learning Research*, 12:2825–2830, 2011.

Jonas Peters, Peter Bühlmann, and Nicolai Meinshausen. Causal inference by using invariant prediction: identification and confidence intervals. *Journal of the Royal Statistical Society: Series B (Statistical Methodology)*, 78(5):947–1012, 2016.

Mohammad Pezeshki, Oumar Kaba, Yoshua Bengio, Aaron C Courville, Doina Precup, and Guillaume Lajoie. Gradient starvation: A learning proclivity in neural networks. *Advances in Neural Information Processing Systems*, 34, 2021.

Geoff Pleiss, Manish Raghavan, Felix Wu, Jon Kleinberg, and Kilian Q Weinberger. On fairness and calibration. *Advances in neural information processing systems*, 30, 2017.

Nasim Rahaman, Aristide Baratin, Devansh Arpit, Felix Draxler, Min Lin, Fred Hamprecht, Yoshua Bengio, and Aaron Courville. On the spectral bias of neural networks. In *International Conference on Machine Learning*, pp. 5301–5310. PMLR, 2019.

Mengye Ren, Wenyuan Zeng, Bin Yang, and Raquel Urtasun. Learning to reweight examples for robust deep learning. In *International conference on machine learning*, pp. 4334–4343. PMLR, 2018.

Marco Tulio Ribeiro, Sameer Singh, and Carlos Guestrin. " why should i trust you?" explaining the predictions of any classifier. In *Proceedings of the 22nd ACM SIGKDD international conference on knowledge discovery and data mining*, pp. 1135–1144, 2016.

Amir Rosenfeld, Richard Zemel, and John K Tsotsos. The elephant in the room. *arXiv preprint arXiv:1808.03305*, 2018.

Elan Rosenfeld, Pradeep Ravikumar, and Andrej Risteski. Domain-adjusted regression or: Erm may already learn features sufficient for out-of-distribution generalization. *arXiv preprint arXiv:2202.06856*, 2022.

Yangjun Ruan, Yann Dubois, and Chris J Maddison. Optimal representations for covariate shift. *arXiv preprint arXiv:2201.00057*, 2021.

Shiori Sagawa, Pang Wei Koh, Tatsunori B Hashimoto, and Percy Liang. Distributionally robust neural networks for group shifts: On the importance of regularization for worst-case generalization. *arXiv preprint arXiv:1911.08731*, 2019.

Shiori Sagawa, Pang Wei Koh, Tony Lee, Irena Gao, Sang Michael Xie, Kendrick Shen, Ananya Kumar, Weihua Hu, Michihiro Yasunaga, Henrik Marklund, et al. Extending the wilds benchmark for unsupervised adaptation. *arXiv preprint arXiv:2112.05090*, 2021.

Luca Scimeca, Seong Joon Oh, Sanghyuk Chun, Michael Poli, and Sangdoo Yun. Which shortcut cues will dnns choose? a study from the parameter-space perspective. *arXiv preprint arXiv:2110.03095*, 2021.

Harshay Shah, Kaustav Tamuly, Aditi Raghunathan, Prateek Jain, and Praneeth Netrapalli. The pitfalls of simplicity bias in neural networks. *Advances in Neural Information Processing Systems*, 33:9573–9585, 2020.

Ali Sharif Razavian, Hossein Azizpour, Josephine Sullivan, and Stefan Carlsson. Cnn features off-the-shelf: an astounding baseline for recognition. In *Proceedings of the IEEE conference on computer vision and pattern recognition workshops*, pp. 806–813, 2014.

Rakshith Shetty, Bernt Schiele, and Mario Fritz. Not using the car to see the sidewalk–quantifying and controlling the effects of context in classification and segmentation. In *Proceedings of the IEEE/CVF Conference on Computer Vision and Pattern Recognition*, pp. 8218–8226, 2019.

Sahil Singla and Soheil Feizi. Salient imagenet: How to discover spurious features in deep learning? *arXiv preprint arXiv:2110.04301*, 2021.

Sahil Singla, Besmira Nushi, Shital Shah, Ece Kamar, and Eric Horvitz. Understanding failures of deep networks via robust feature extraction. In *Proceedings of the IEEE/CVF Conference on Computer Vision and Pattern Recognition*, pp. 12853–12862, 2021.

Nimit Sohoni, Jared Dunnmon, Geoffrey Angus, Albert Gu, and Christopher Ré. No subclass left behind: Fine-grained robustness in coarse-grained classification problems. *Advances in Neural Information Processing Systems*, 33:19339–19352, 2020.

Nimit Sohoni, Maziar Sanjabi, Nicolas Ballas, Aditya Grover, Shaoliang Nie, Hamed Firooz, and Christopher Ré. Barack: Partially supervised group robustness with guarantees. *arXiv preprint arXiv:2201.00072*, 2021.

Chen Sun, Abhinav Shrivastava, Saurabh Singh, and Abhinav Gupta. Revisiting unreasonable effectiveness of data in deep learning era. In *Proceedings of the IEEE international conference on computer vision*, pp. 843–852, 2017.

Enzo Tartaglione, Carlo Alberto Barbano, and Marco Grangetto. End: Entangling and disentangling deep representations for bias correction. In *Proceedings of the IEEE/CVF conference on computer vision and pattern recognition*, pp. 13508–13517, 2021.

Damien Teney, Ehsan Abbasnejad, Simon Lucey, and Anton van den Hengel. Evading the simplicity bias: Training a diverse set of models discovers solutions with superior ood generalization. *arXiv preprint arXiv:2105.05612*, 2021a.

Damien Teney, Ehsan Abbasnejad, and Anton van den Hengel. Unshuffling data for improved generalization in visual question answering. In *Proceedings of the IEEE/CVF International Conference on Computer Vision*, pp. 1417–1427, 2021b.

Prasetya Ajie Utama, Nafise Sadat Moosavi, and Iryna Gurevych. Towards debiasing nlu models from unknown biases. *arXiv preprint arXiv:2009.12303*, 2020.

Victor Veitch, Alexander D'Amour, Steve Yadlowsky, and Jacob Eisenstein. Counterfactual invariance to spurious correlations: Why and how to pass stress tests. *arXiv preprint arXiv:2106.00545*, 2021.

Pauli Virtanen, Ralf Gommers, Travis E. Oliphant, Matt Haberland, Tyler Reddy, David Cournapeau, Evgeni Burovski, Pearu Peterson, Warren Weckesser, Jonathan Bright, Stéfan J. van der Walt, Matthew Brett, Joshua Wilson, K. Jarrod Millman, Nikolay Mayorov, Andrew R. J. Nelson, Eric Jones, Robert Kern, Eric Larson, C J Carey, İlhan Polat, Yu Feng, Eric W. Moore, Jake VanderPlas, Denis Laxalde, Josef Perktold, Robert Cimrman, Ian Henriksen, E. A. Quintero, Charles R. Harris, Anne M. Archibald, Antônio H. Ribeiro, Fabian Pedregosa, Paul van Mulbregt, and SciPy 1.0 Contributors. SciPy 1.0: Fundamental Algorithms for Scientific Computing in Python. *Nature Methods*, 17:261–272, 2020. doi: 10.1038/s41592-019-0686-2.

Catherine Wah, Steve Branson, Peter Welinder, Pietro Perona, and Serge Belongie. The caltech-ucsd birds-200-2011 dataset. 2011.

Haohan Wang, Zexue He, Zachary C Lipton, and Eric P Xing. Learning robust representations by projecting superficial statistics out. *arXiv preprint arXiv:1903.06256*, 2019.

Thomas Wolf, Lysandre Debut, Victor Sanh, Julien Chaumond, Clement Delangue, Anthony Moi, Pierric Cistac, Tim Rault, Rémi Louf, Morgan Funtowicz, et al. Huggingface's transformers: State-of-the-art natural language processing. *arXiv preprint arXiv:1910.03771*, 2019.

Han Xiao, Kashif Rasul, and Roland Vollgraf. Fashion-mnist: a novel image dataset for benchmarking machine learning algorithms, 2017.

Kai Xiao, Logan Engstrom, Andrew Ilyas, and Aleksander Madry. Noise or signal: The role of image backgrounds in object recognition. *arXiv preprint arXiv:2006.09994*, 2020.

Yilun Xu, Hao He, Tianxiao Shen, and Tommi S. Jaakkola. Controlling directions orthogonal to a classifier. In *International Conference on Learning Representations*, 2022.

Yadollah Yaghoobzadeh, Soroush Mehri, Remi Tachet, Timothy J Hazen, and Alessandro Sordoni. Increasing robustness to spurious correlations using forgettable examples. *arXiv preprint arXiv:1911.03861*, 2019.

John R Zech, Marcus A Badgeley, Manway Liu, Anthony B Costa, Joseph J Titano, and Eric Karl Oermann. Variable generalization performance of a deep learning model to detect pneumonia in chest radiographs: a cross-sectional study. *PLoS medicine*, 15(11):e1002683, 2018.

Xiaohua Zhai, Joan Puigcerver, Alexander Kolesnikov, Pierre Ruyssen, Carlos Riquelme, Mario Lucic, Josip Djolonga, Andre Susano Pinto, Maxim Neumann, Alexey Dosovitskiy, et al. A large-scale study of representation learning with the visual task adaptation benchmark. *arXiv preprint arXiv:1910.04867*, 2019.

Jianguo Zhang, Marcin Marszałek, Svetlana Lazebnik, and Cordelia Schmid. Local features and kernels for classification of texture and object categories: A comprehensive study. *International journal of computer vision*, 73(2):213–238, 2007.

Jingzhao Zhang, Aditya Menon, Andreas Veit, Srinadh Bhojanapalli, Sanjiv Kumar, and Suvrit Sra. Coping with label shift via distributionally robust optimisation. *arXiv preprint arXiv:2010.12230*, 2020.

Michael Zhang, Nimit S Sohoni, Hongyang R Zhang, Chelsea Finn, and Christopher Ré. Correct-n-contrast: A contrastive approach for improving robustness to spurious correlations. *arXiv preprint arXiv:2203.01517*, 2022.

Bolei Zhou, Agata Lapedriza, Aditya Khosla, Aude Oliva, and Antonio Torralba. Places: A 10 million image database for scene recognition. *IEEE transactions on pattern analysis and machine intelligence*, 40(6):1452–1464, 2017.

Wei Zhu, Haitian Zheng, Haofu Liao, Weijian Li, and Jiebo Luo. Learning bias-invariant representation by cross-sample mutual information minimization. In *Proceedings of the IEEE/CVF International Conference on Computer Vision*, pp. 15002–15012, 2021.

APPENDIX OUTLINE

This appendix is organized as follows. In Section A we provide additional related work discussion. In Section B we present details on the experiments on feature learning in the presence of spurious correlations. In Section C we provide details on the results for the spurious correlation benchmark datasets. We provide details on the experiments on the reliance of ImageNet-trained models on the background in Section D and on the texture-bias in Section E. In Section F we provide further discussion of the results presented in the paper and future work.

Code references. In addition to the experiment-specific packages that we discuss throughout the appendix, we used the following libraries and tools in this work: NumPy (Harris et al., 2020), SciPy (Virtanen et al., 2020), PyTorch (Paszke et al., 2017), Jupyter notebooks (Kluyver et al., 2016), Matplotlib (Hunter, 2007), Pandas (McKinney, 2010), transformers (Wolf et al., 2019).

A ADDITIONAL RELATED WORK

Other group robustness methods. Another group of papers proposes regularization techniques to learn diverse solutions on the train data, focusing on different groups of features (Teney et al., 2021a; Lee et al., 2022; Pagliardini et al., 2022; Pezeshki et al., 2021). Xu et al. (2022) show how to train *orthogonal classifiers*, i.e. classifiers invariant to given spurious features in the data. Other papers proposed methods based on meta-learning the weights for a weighted loss (Ren et al., 2018) and group-agnostic adaptive regularization (Cao et al., 2019; 2020). Sohoni et al. (2020) use clustering of internal features to provide approximate labels for group distributionally robust optimization. A number of prior works address de-biasing classifiers by leveraging prior knowledge on the bias type (Li & Vasconcelos, 2019; Kim et al., 2019; Tartaglione et al., 2021; Teney et al., 2021b; Zhu et al., 2021; Wang et al., 2019; Cadene et al., 2019; Li et al., 2018b).

Spurious correlations in natural image datasets. Multiple works demonstrated that natural image datasets contain spurious correlations that hurt neural network models (Kolesnikov & Lampert, 2016; Xiao et al., 2020; Shetty et al., 2019; Alcorn et al., 2019; Singla & Feizi, 2021; Singla et al., 2021; Moayeri et al., 2022). Notably, Geirhos et al. (2018) demonstrated that ImageNet-trained CNNs are biased towards texture rather than shape of the objects. Follow-up work explored this texture bias and showed that despite being texture-biased, CNNs still often represent information about the shape in their feature representations (Hermann et al., 2020; Islam et al., 2021). In Section 7 we show that it is possible to reduce the reliance of ImageNet-trained models on background context and texture information by retraining just the last layer of the model.

Transfer learning. Transfer learning (Pan & Yang, 2009; Sharif Razavian et al., 2014) is an extremely popular framework in modern machine learning. Multiple works demonstrate its effectiveness (e.g. Girshick, 2015; Huh et al., 2016; He et al., 2017; Sun et al., 2017; Mahajan et al., 2018; Kolesnikov et al., 2020; Maddox et al., 2021), and study when and why transfer learning can be effective (Zhai et al., 2019; Neyshabur et al., 2020; Abnar et al., 2021; Kornblith et al., 2019; Kumar et al., 2022). Bommasani et al. (2021) provide a comprehensive discussion of modern transfer learning with large-scale models. While algorithmically our proposed DFR method is related to transfer learning, it has a different motivation and works on different problems. We discuss the relation between DFR and transfer learning in detail in Section 5.

Related methods have been developed in several areas of machine learning, such as ML Fairness (Dwork et al., 2012; Hardt et al., 2016; Kleinberg et al., 2016; Pleiss et al., 2017; Agarwal et al., 2018; Khani et al., 2019), NLP (McCoy et al., 2019; Lovering et al., 2020; Kaushik et al., 2020; 2021; Eisenstein, 2022; Veitch et al., 2021) domain adaptation (Ganin & Lempitsky, 2015; Ganin et al., 2016) and domain generalization (Blanchard et al., 2011; Muandet et al., 2013; Li et al., 2018a; Gulrajani & Lopez-Paz, 2020; Ruan et al., 2021) including works on Invariant Risk Minimization and causality (Peters et al., 2016; Arjovsky et al., 2019; Krueger et al., 2021; Aubin et al., 2021).

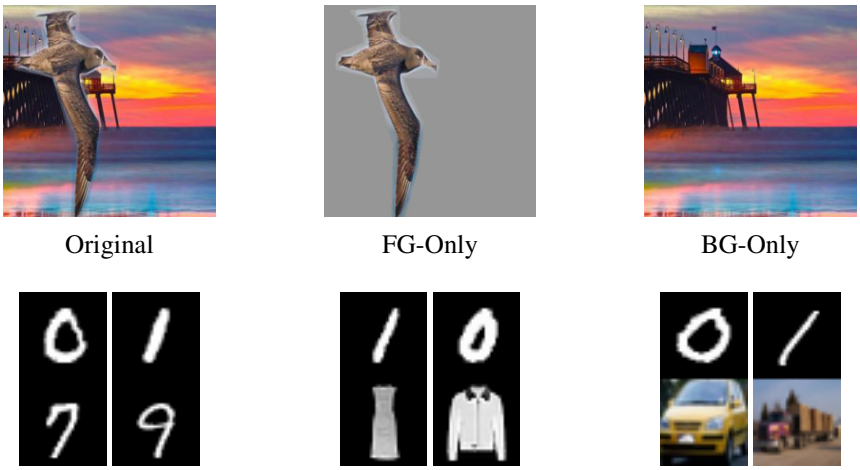

Figure 4: **Data examples.** Variations of the waterbirds (Top) and Dominoes (Bottom) datasets generated for the experiment in Section 4.

B Details: Understanding Representation Learning with Spurious Correlations

Here we provide details on the experiments in Section 4.

B.1 Feature learning on Waterbirds

Inverse problem. In Table 4 we present the results on the inverted Waterbirds problem, where the goal is to predict the background type while the bird type serves as a spurious feature. We note that prior work did not consider this reverse Waterbirds problem. The results for the inverted problem are analogous to the results for the standard Waterbirds (Table 1): models trained on the Original data learn the background features sufficiently well to predict the background type with high accuracy when the spurious foreground feature is not present, but perform poorly when presented with conflicting background and foreground features. While it is often suggested than neural networks are biased to learn the background (Xiao et al., 2020), we see that in fact the network relies on the spurious foreground feature (bird) when trained to predict the background.

Data. We show examples of Original, FG-Only and BG-Only Waterbirds images in Figure 4. To generate the data, we follow the instructions at `github.com/kohpangwei/group_DRO#waterbirds`, but in addition to the Original data we save the backgrounds and foregrounds separately. Consequently, the FG-Only data contains the same exact birds images as the Original data, and the BG-Only data contains the same exact places images as the Original data. For the 100% spurious correlation strength we simply discard all the minority groups data from the Original (95% spurious correlation) training dataset. For the Balanced data, we start with the Original data with 95% spurious correlation and replaced the background in the smallest possible number of images (chosen randomly) to achieve a 50% spurious correlation strength.

Hyper-parameters. For the experiments in this section we use a ResNet-50 model pretrained on ImageNet, imported from the `torchvision` package: `torchvision.models.resnet50(pretrained=True)` (Marcel & Rodriguez, 2010). We train the models for 50 epochs with SGD with a constant learning rate of 10^{-3}, momentum decay of 0.9, batch size 32 and a weight decay of 10^{-2}. We use random crops (`RandomResizedCrop(224, scale=(0.7, 1.0), ratio=(0.75, 4./3.), interpolation=2)`) and horizontal flips (`RandomHorizontalFlip()`) implemented in `torchvision.transforms` as data augmentation.

B.2 Dominoes datasets

Data. We show data examples from Dominoes datasets (MNIST-MNIST, MNIST-FashionMNIST and MNIST-CIFAR) in Figure 4. The top half of each image shows MNIST digits from classes

Train Data	Spurious Corr. (%)	Test Data (Worst/Mean, %)	
		Original	BG-Only
Balanced	50	93.2/95.6	93.6/96.0
Original	95	77.4/91.2	93.1/95.7
Original	100	36.1/77.5	92.7/94.8
Place-Only	-	91.8/94.2	92.4/95.2

Table 4: **Feature learning on Inverted Waterbirds.** ERM classifiers trained on Inverted Waterbirds with Original and BG-Only images. Here the target is associated with the background type, and the foreground (bird type) serves as the spurious feature. All the models trained on the Original data including the model trained without any minority group examples (*Spurious corr.* 100%) underperform on the worst-group accuracy on the Original data, but perform well on the BG-Only data, almost matching the performance of the BG-Only trained model.

$\{0, 1\}$, and the bottom half shows: MNIST images from classes {7, 9} for MNIST-MNIST, Fashion-MNIST images from classes {coat, dress} for MNIST-FashionMNIST, and CIFAR-10 images from classes {car, truck} for MNIST-CIFAR. The label corresponds to the more complex bottom part of the image, but the top and bottom parts are correlated (we consider 95%, 99% and 100% levels of spurious correlation strength in experiments). 20% of the training data was reserved for validation or *reweighting* dataset (see Section 5) where each group is equally represented.

Hyper-parameters. We used a randomly initialized ResNet-20 architecture for this set of experiments. We trained the network for 500 epochs with SGD with batch size 32, weight decay 10^{-3}, initial learning rate value 10^{-2} and a cosine annealing learning rate schedule. For the logistic regression model, we first extract the embeddings from the penultimate layer of the network, then use the logistic regression implementation (`sklearn.linear_model.LogisticRegression`) from the `scikit-learn` package (Pedregosa et al., 2011). We use ℓ_1 regularization and tune the inverse regularization strength parameter C in the range $\{0.1, 10, 100, 1000\}$. For more details on Deep Feature Reweighting implementation and tuning, see section C.

Transfer from simple to complex features. In addition to the results presented in Figure 2, we measure the decoded accuracy using the model trained just on the spurious simple features: the top half of the image showing an MNIST digit. After training, we retrain the last layer of the model using a validation split of the corresponding Dominoes dataset which has both top and bottom parts. In this case, we measure the transfer learning performance with the features learned on the binary MNIST classification problem applied to the more complex bottom half of the image. We obtain the following *transfer accuracy* results: 92.5% on MNIST-MNIST, 92.1% on MNIST-Fashion and 61.4% on MNIST-CIFAR. On all datasets, the decoded accuracy reported in Figure 2 for the spurious correlation levels 99% and 95% is better than the transfer accuracy. For the 100% spurious correlation, transfer achieves comparable results on MNIST-Fashion and MNIST-CIFAR, but on MNIST-MNIST the decoded accuracy with a model trained on the data with the core feature is significantly higher (99% vs 92%). These results confirm that for the spurious correlation strength below 100%, the model learns a high quality representation of the core features, which cannot be explained by transfer learning from the spurious feature.

B.3 ColorMNIST

Data. We follow Zhang et al. (2022) to generate ColorMNIST dataset: there are 5 classes corresponding to pairs of digits $(0, 1), (2, 3), (4, 5), (6, 7), (8, 9)$, and 5 fixed colors such that in train data each class y has a color s which is associated with it with correlation p_{corr}, and the remaining examples are colored with the remaining colors uniformly at random. Validation split is a randomly sampled 10% fraction of the original MNIST data, and validation and test data exmaples are colored with 5 colors uniformly at random.

Hyper-parameters. We train a small LeNet-like Convolutional Neural Network model on this dataset varying p_{corr}. The model is trained for 5 epochs, with batch size 32, learning rate 10^{-3}, and weight decay 5×10^{-4}, following Zhang et al. (2022). CNN consists of 2 convolutional layers with 6 and 16 output filters, followed by a max pooling layer, then another convolutional layer with 32 output filters and a fully-connected layer.

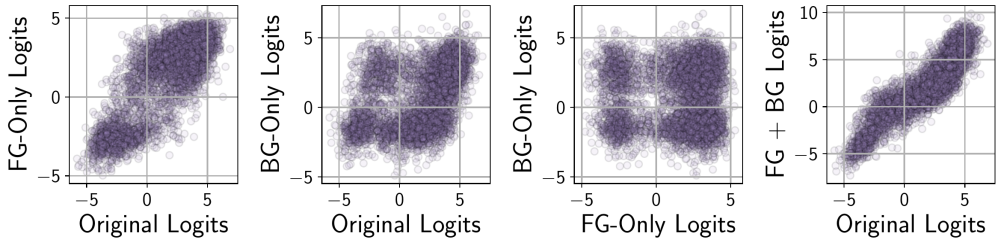

Figure 5: **Logit additivity.** Distribution of logits for the negative class on the test data for a model trained on Waterbirds dataset. We show scatter plots of the logits for the Original, FG-Only and BG-Only images. The logits on Original images are well aligned with sums of logits on the corresponding FG and BG images (rightmost panel), suggesting that the foreground and background features are processed close to independently in the network.

p_{corr}	no corr.	0.8	0.9	0.95	0.995	1.0
ERM	$94.5_{\pm 1.0}$	$85.1_{\pm 2.2}$	$66.0_{\pm 7.2}$	$40.8_{\pm 3.6}$	$0.0_{\pm 0.0}$	$0.0_{\pm 0.0}$
$\text{DFR}^{\text{Val}}_{\text{Tr}}$	–	$93.8_{\pm 0.9}$	$92.6_{\pm 0.7}$	$91.6_{\pm 0.8}$	$80.4_{\pm 1.1}$	$77.3_{\pm 1.3}$

Table 5: **Results on ColorMNIST.** Worst-group accuracy of a small CNN model trained on 5-class ColorMNIST dataset, varying the spurious correlation strength p_{corr} between classes and colors. DFR achieves strong performance even in the challenging settings with strong correlation between class labels and colors. We report mean $\pm$ std over 3 independent runs of the method.

We report worst-group accuracy for ERM and $\text{DFR}^{\text{Val}}_{\text{Tr}}$ in Table 5. The *no corr.* results for ERM correspond to the model trained on the dataset without correlation between colors and class labels. Notably, DFR recovers strong worst-group performance even in the cases when base model has 0% worst-group accuracy ($p_{corr} = 1.0$ and $p_{corr} = 0.995$). For $p_{corr} < 0.95$ DFR's worst-group accuracy is closely matching the optimal accuracy of the model trained on data without spurious correlations.

B.4 Logit additivity

To better understand why the models trained on the Original Waterbirds data perform well on FG-Only images, in Figure 5 we inspect the logits of a trained model. We show scatter plots of logits for the negative class (logits for the positive class behave analogously) on the Original, FG-Only and BG-Only test data. Both logits on FG-Only and BG-Only data correlate with the logits on the Original images, and FG-Only show a higher correlation. The FG-Only and BG-Only logits are not correlated with each other, as in test data the groups are balanced and the foreground and background are independent.

We find that the sum of the logits for the BG-Only and the logits for the FG-Only images provides a good approximation of the logits on the corresponding Original image (combining the foreground and the background). We term this phenomenon *logit additivity*: on Waterbirds, logits for the different predictive features (both core and spurious) are computed close to independently and added together in the last classification layer.

Waterbirds dataset				
	$\mathcal{G}_1$	$\mathcal{G}_2$	$\mathcal{G}_3$	$\mathcal{G}_4$
Image Examples			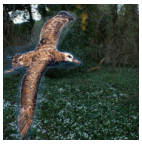	
Description	landbird on land	landbird on water	waterbird on land	waterbird on water
Class Label	0	0	1	1
# Train data	3498 (73%)	184 (4%)	56 (1%)	1057 (22%)
# Val data	467	466	133	133
Target: bird type; **Spurious feature**: background type; **Minority**: $\mathcal{G}_2, \mathcal{G}_3$				

CelebA hair color dataset				
	$\mathcal{G}_1$	$\mathcal{G}_2$	$\mathcal{G}_3$	$\mathcal{G}_4$
Image Examples				
Description	Non-blond woman	Non-blond man	Blond woman	Blond man
Class Label	0	0	1	1
# Train data	71629 (44%)	66874 (41%)	22880 (14%)	1387 (1%)
# Val data	8535	8276	2874	182
Target: hair color; **Spurious feature**: gender; **Minority**: $\mathcal{G}_4$				

Figure 6: **Waterbirds and CelebA data.** Dataset descriptions and example images from each group on Waterbirds and CelebA datasets.

C Details: Spurious Correlation Benchmarks

Here we provide details and additional ablations on the experiments in Section 6.

Data. We use the standard Waterbirds, CelebA and MultiNLI datasets, following e.g. (Sagawa et al., 2019; Liu et al., 2021; Idrissi et al., 2021). We use CivilComments dataset as implemented in the WILDS benchmark (Koh et al., 2021). See Figures 6, 7 for group descriptions and data examples.

Base model hyper-parameters. For the experiments on Waterbirds and CelebA we use a ResNet-50 model pretrained on ImageNet, imported from the `torchvision` package: `torchvision.models.resnet50(pretrained=True)`. We use random crops (`RandomResizedCrop(224, scale=(0.7, 1.0), ratio=(0.75, 4./3.), interpolation=2)`) and horizontal flips (`RandomHorizontalFlip()`) implemented in `torchvision.transforms` as data augmentation. We train all models with SGD with momentum decay of 0.9 and a constant learning rate. On Waterbirds, we train the models for 100 epochs with weight decay 10^{-3}, learning rate 10^{-3} and batch size 32. On CelebA, we train the models for 50 epochs with weight decay 10^{-4}, learning rate 10^{-3} and batch size 128. We do not use early stopping. On MultiNLI and CivilComments, we use the BERT for classification model from the `transformers` package: `BertForSequenceClassification.from_pretrained('bert-base-uncased', num_labels=num_classes)`. We train the BERT models with the AdamW (Loshchilov & Hutter, 2017) with linear learning rate annealing with initial learning rate 10^{-5}, batch size 16 and weight decay 10^{-4} for 5 epochs.

DFR details. For DFR, we first extract and save the embeddings (inputs to the classification layer of the base model) of the training, validation and testing data using the base model. We then preprocess the embeddings to have zero mean and unit standard deviation using the standard scaler `sklearn.preprocessing.StandardScaler` from the `scikit-learn` package. In each case, we compute the preprocessing statistics on the reweighting data used to train the last layer. To retrain the last layer, we use the logistic regression implementation (`sklearn.linear_model.LogisticRegression`) from the `scikit-learn` package. We use ℓ_1 regularization. For $\text{DFR}^{\text{Val}}_{\text{Tr}}$ we only tune the inverse regularization strength parame-

MultiNLI

	Text examples	Class label	Description	# Train data	# Val data
$\mathcal{G}_1$	*"if residents are unhappy, they can put wheels on their homes and go someplace else, she said. [SEP] residents are stuck here but they can't go anywhere else."*	0	contradiction no negations	57498 (28%)	22814
$\mathcal{G}_2$	*"within this conflict of values is a clash about art. [SEP] there is no clash about art."*	0	contradiction has negations	11158 (5%)	4634
$\mathcal{G}_3$	*"there was something like amusement in the old man's voice. [SEP] the old man showed amusement."*	1	entailment no negations	67376 (32%)	26949
$\mathcal{G}_4$	*"in 1988, the total cost for the postal service was about $36. [SEP] the postal service cost us citizens almost nothing in the late 80's. "*	1	entailment has negations	1521 (1%)	613
$\mathcal{G}_5$	*"yeah but even even cooking over an open fire is a little more fun isn't it [SEP] i like the flavour of the food."*	2	neutral no negations	66630 (32%)	26655
$\mathcal{G}_6$	*"that's not too bad [SEP] it's better than nothing"*	2	neutral has negations	1992 (1%)	797

Target: contradiction / entailment / neutral; **Spurious feature**: has negation words. **Minority**: $\mathcal{G}_4$, $\mathcal{G}_6$

CivilComments

Text examples	Class label	Description	# Train data	# Val data
"I'm quite surprised this worked for you. Infrared rays cannot penetrate tinfoil."	0	non-toxic no identities	148186 (55%)	25159
"I think you may have misunderstood what 'straw men' are. But I'm glad that your gravy is good."	0	non-toxic has identities	90337 (33%)	14966
"Hahahaha putting his faith in Snopes. Pathetic."	1	toxic no identities	12731 (5%)	2111
"That sounds like something a white person would say."'	1	toxic has identities	17784 (7%)	2944

Target: Toxic / not toxic comment; **Spurious feature**: mentions protected categories.

Figure 7: **MultiNLI and CivilComments data.** Dataset descriptions and data examples from different groups on MultiNLI and CivilComments. We underline the words corresponding to the spurious feature. CivilComments contains 16 overlapping groups (corresponding to toxic / non-toxic comments and mentions of one of the protected identities: male, female, LGBT, black, white, Christian, Muslim, other religion. We only show examples with mentions of the male and white identities.

Method	ImageNet Pretrain	Dataset Fine-tune	Waterbirds		CelebA	
			Worst(%)	Mean(%)	Worst(%)	Mean(%)
Base Model	✓	✓	$74.9_{\pm 2.4}$	$98.1_{\pm 0.1}$	$46.9_{\pm 2.8}$	$95.3_{\pm 0}$
$\text{DFR}^{\text{Tr}}_{\text{Tr}}$	✓	✓	$90.2_{\pm 0.8}$	$97.0_{\pm 0.3}$	$80.7_{\pm 2.4}$	$85.4_{\pm 0.4}$
$\text{DFR}^{\text{Val}}_{\text{Tr}}$	✓	✓	$92.9_{\pm 0.2}$	$94.2_{\pm 0.4}$	$88.3_{\pm 1.1}$	$89.6_{\pm 0.4}$
Base Model	✗	✓	$6.9_{\pm 3.0}$	$88.0_{\pm 1.1}$	$39.8_{\pm 2.0}$	$95.7_{\pm 0.1}$
$\text{DFR}^{\text{Tr}}_{\text{Tr}}$	✗	✓	$45.4_{\pm 4.1}$	$69.8_{\pm 7.0}$	$83.4_{\pm 2.6}$	$87.5_{\pm 0.3}$
$\text{DFR}^{\text{Val}}_{\text{Tr}}$	✗	✓	$53.9_{\pm 1.8}$	$62.6_{\pm 2.2}$	$85.0_{\pm 2.1}$	$87.6_{\pm 0.3}$
$\text{DFR}^{\text{Val}}_{\text{IN}}$	✓	✗	$88.7_{\pm 0.4}$	$89.7_{\pm 0.1}$	$73.1_{\pm 2.6}$	$80.9_{\pm 0.5}$

Table 6: **Effect of ImageNet pretraining and dataset fine-tuning.** Results for DFR on the Waterbirds and CelebA datasets when using an ImageNet-trained model as a feature extractor, training the feature extractor from random initialization or initializing the feature extractor with ImageNet-trained weights and fine-tuning on the target data. On Waterbirds, we can achieve surprisingly strong worst group accuracy of 88.7% without finetuning on the target data. On CelebA, we can achieve reasonable worst group accuracy of 85% without pretraining. However, on both datasets, both ImageNet pretraining and dataset finetuning are needed to achieve optimal performance. All methods in Table 2 use ImageNet-trained models as initialization and finetune on the target dataset.

Retrained	WB	CelebA
Last Layer	$93.1_{\pm 0.2}$	$88.3_{\pm 0.5}$
Last 2 Layers	$93.1_{\pm 0.5}$	$87.2_{\pm 0.9}$
Last Block	$90.7_{\pm 0.4}$	$83.0_{\pm 0.9}$
All Layers	$35.6_{\pm 0.1}$	$77.8_{\pm 0.1}$

Table 7: **Retraining multiple layers.** We retrain the last linear layer, last two layers (linear, last batchnorm and conv), last residual block, and all layers from scratch on group-balanced validation data. Retraining the last layer is sufficient for optimal performance, and moreover retraining more layers can hurt the results.

ter C: we consider the values in range $\{1., 0.7, 0.3, 0.1, 0.07, 0.03, 0.01\}$ and select the value that leads to the best worst-group performance on the available validation data (as described in Section 6, for $\text{DFR}^{\text{Val}}_{\text{Tr}}$ we use half of the validation to train the logistic regression model and the other half to tune the parameters at the tuning stage). For $\text{DFR}^{\text{Tr}}_{\text{Tr}}$ we additionally tune the class weights: we set the weight for one of the classes to 1 and consider the weights for the other class in range $\{1, 2, 3, 10, 100, 300, 1000\}$; we then switch the classes and repeat the procedure. For the final evaluation, we use the best values of the hyper-parameters obtained during the tuning phase and train a logistic regression model on all of the available reweighting data. We train the logistic regression model on the reweighting data 10 times with random subsets of the data (we take all of the data from the smallest group, and subsample the other groups randomly to have the same number of datapoints) and average the weights of the learned models. We report the model with averaged weights.

Is ImageNet pretraining necessary for image benchmarks? DFR relies on the ability of the feature extractor to learn diverse features, which may suggest that ImageNet pretraining is crucial. In Appendix Table 6, we report the results on the same problems, but training the feature extractor from scratch. We find that on Waterbirds, ImageNet pretraining indeed has a dramatic effect on the performance of DFR as well as the base feature extractor model. However, on CelebA DFR shows strong performance regardless of pretraining. The difference between Waterbirds and CelebA is that Waterbirds contains only $4.8k$ training points, making it difficult to learn a meaningful feature extractor from scratch. Furthermore, on both datasets, finetuning the feature extractor on the target data is crucial: just using the features extracted by an ImageNet-trained model leads to poor results. We note that all the baselines considered in Table 2 use ImageNet pretraining.

Retraining multiple layers. In Table 7 we perform another ablation by retraining multiple layers from scratch on the group-balanced validation dataset on Waterbirds and CelebA. We find that

Base Model Hypers				Method	Waterbirds	
lr	wd	batch size	aug		Worst(%)	Mean(%)
10^{-3}	10^{-3}	32	✓	Base Model	$74.9_{\pm 2.4}$	$98.1_{\pm 0.1}$
				$\text{DFR}_{\text{Tr}}^{\text{Val}}$	$92.9_{\pm 0.2}$	$94.2_{\pm 0.4}$
10^{-3}	10^{-3}	32	✗	Base Model	73.4	97.7
				$\text{DFR}_{\text{Tr}}^{\text{Val}}$	90.9	92.2
10^{-3}	10^{-2}	32	✓	Base Model	24.1	94.4
				$\text{DFR}_{\text{Tr}}^{\text{Val}}$	88.0	88.6
10^{-3}	10^{-2}	32	✗	Base Model	66.4	97.1
				$\text{DFR}_{\text{Tr}}^{\text{Val}}$	90.1	90.5
$3 \cdot 10^{-3}$	10^{-3}	32	✓	Base Model	71.5	98.1
				$\text{DFR}_{\text{Tr}}^{\text{Val}}$	91.9	93.5
$3 \cdot 10^{-3}$	10^{-3}	32	✗	Base Model	76.5	98.0
				$\text{DFR}_{\text{Tr}}^{\text{Val}}$	89.5	94.5
10^{-3}	10^{-3}	64	✓	Base Model	73.5	98.0
				$\text{DFR}_{\text{Tr}}^{\text{Val}}$	93.1	95.0
10^{-3}	10^{-3}	64	✗	Base Model	69.5	97.4
				$\text{DFR}_{\text{Tr}}^{\text{Val}}$	89.0	93.6

Base Model Hypers				Method	CelebA	
lr	wd	batch size	aug		Worst(%)	Mean(%)
10^{-3}	10^{-4}	128	✓	Base Model	$46.9_{\pm 2.8}$	$95.3_{\pm 0}$
				$\text{DFR}_{\text{Tr}}^{\text{Val}}$	$88.3_{\pm 1.1}$	$91.3_{\pm 0.3}$
10^{-3}	10^{-3}	128	✓	Base Model	$44.3_{\pm 6.4}$	$95.2_{\pm 0.1}$
				$\text{DFR}_{\text{Tr}}^{\text{Val}}$	$86.2_{\pm 1.2}$	$90.8_{\pm 0.7}$
10^{-3}	10^{-4}	128	✗	Base Model	$46.7_{\pm 0.0}$	$95.3_{\pm 0.1}$
				$\text{DFR}_{\text{Tr}}^{\text{Val}}$	$86.9_{\pm 1.1}$	$91.6_{\pm 0.2}$
10^{-3}	10^{-3}	128	✗	Base Model	$40.6_{\pm 8.7}$	$95.1_{\pm 0.2}$
				$\text{DFR}_{\text{Tr}}^{\text{Val}}$	$85.6_{\pm 1.4}$	$91.8_{\pm 0.5}$

Table 8: **Effect of base model hyper-parameters.** We report the results of $\text{DFR}_{\text{Tr}}^{\text{Val}}$ for a range of base model hyper-parameters on Waterbirds and CelebA as well as the performance of the corresponding base models. While the quality of the base model has an effect on DFR, the results are fairly robust. For a subset of configurations we report the mean and standard deviation over 3 independent runs of the base model and DFR.

retraining just the last layer provides optimal performance, retraining the last two layers (the last convolutional layer and the fully-connected classifier layer) or the last residual block is competitive (but worse), while retraining the full network is a lot worse.

Method	Group Info	Waterbirds		CelebA		MultiNLI		CivilComments	
	Train / Val	Worst(%)	Mean(%)	Worst(%)	Mean(%)	Worst(%)	Mean(%)	Worst(%)	Mean(%)
Base (ERM)	✗ / ✗	$74.9_{\pm 2.4}$	$98.1_{\pm 0.1}$	$46.9_{\pm 2.8}$	$95.3_{\pm 0}$	$65.9_{\pm 0.3}$	$82.8_{\pm 0.1}$	$55.6_{\pm 0.6}$	$92.1_{\pm 0.1}$
$\text{DFR}^{\text{Tr}}_{\text{Tr}}$	✓ / ✓	$90.2_{\pm 0.8}$	$97.0_{\pm 0.3}$	$80.7_{\pm 2.4}$	$90.6_{\pm 0.7}$	$71.5_{\pm 0.6}$	$82.5_{\pm 0.2}$	$58.0_{\pm 1.3}$	$92.0_{\pm 0.1}$
$\text{DFR}^{\text{Val}}_{\text{Tr}}$	✗ / ✓✓	$\mathbf{92.9}_{\pm 0.2}$	$94.2_{\pm 0.4}$	$88.3_{\pm 1.1}$	$91.3_{\pm 0.3}$	$\mathbf{74.7}_{\pm 0.7}$	$82.1_{\pm 0.2}$	$\mathbf{70.1}_{\pm 0.8}$	$87.2_{\pm 0.3}$
Base Model trained without minority groups									
Base (ERM)	✗ / ✗	$31.9_{\pm 3.6}$	$96.0_{\pm 0.2}$	$21.7_{\pm 3.2}$	$95.2_{\pm 0.1}$	$66.0_{\pm 1.6}$	$82.5_{\pm 0.1}$	$8.4_{\pm 4.9}$	$73.8_{\pm 0.3}$
$\text{DFR}^{\text{Tr}}_{\text{Tr-NM}}$	✓ / ✓	$89.9_{\pm 0.6}$	$94.3_{\pm 0.5}$	$\mathbf{89.0}_{\pm 1.1}$	$91.6_{\pm 0.4}$	$73.0_{\pm 0.6}$	$82.2_{\pm 0.1}$	$66.5_{\pm 0.7}$	$85.9_{\pm 0.3}$

Table 9: **DFR variations.** Worst-group and mean test accuracy of DFR variations on the benchmark datasets problems. $\text{DFR}^{\text{Val}}_{\text{Tr}}$ achieves the best performance across the board. Interestingly, $\text{DFR}^{\text{Tr}}_{\text{Tr-NM}}$ outperforms $\text{DFR}^{\text{Tr}}_{\text{Tr}}$ on all dataset and even outperforms $\text{DFR}^{\text{Val}}_{\text{Tr}}$ on CelebA. For all experiments, we report mean$\pm$std over 5 independent runs of the method.

What if we just use ImageNet features? As a baseline, we apply DFR to features extracted by a model pretrained on ImageNet with no fine-tuning on CelebA and Waterbirds data. We report the results in Table 6 ($\text{DFR}^{\text{Tr}}_{\text{IN}}$ and $\text{DFR}^{\text{Val}}_{\text{IN}}$ lines). While on Waterbirds the performance is fairly good, on CelebA finetuning is needed to get reasonable performance. The results in Table 6 suggest that both ImageNet pretraining and fine-tuning on the target data are needed to train the best feature extractor for DFR.

Robustness to base model hyper-parameters In Table 8 we report the results of $\text{DFR}^{\text{Val}}_{\text{Tr}}$ for a range of configurations of the baseline model hyper-parameters. While the quality of the base model clearly has an effect on DFR performance, we achieve competitive results for all the hyper-parameter configurations that we consider, even when the base model performs poorly. For example, on Waterbirds with data augmentation, learning rate 10^{-3} and weight decay 10^{-2} the base model achieves worst group accuracy of 24.1%, but by retraining the last layer of this model with $\text{DFR}^{\text{Val}}_{\text{Tr}}$ we still achieve 88% worst group accuracy.

C.1 Prior work assumptions

In Section 6 we compare DFR to ERM, Group DRO (Sagawa et al., 2019), JTT (Liu et al., 2021), CnC (Zhang et al., 2022), SUBG (Idrissi et al., 2021) and SSA (Nam et al., 2022). These methods differ in assumptions about the amount of group information available.

Group DRO and SUBG assume that both train and validation data have group labels, and the hyper-parameters are tuned using worst-group validation accuracy. $\text{DFR}^{\text{Tr}}_{\text{Tr}}$ and $\text{DFR}^{\text{Tr}}_{\text{Tr-NM}}$ match the setting of these methods and use the same data and group information; in particular, these methods only use the validation set with group labels to tune the hyper-parameters.

A number of prior works (e.g. Liu et al., 2021; Creager et al., 2021; Zhang et al., 2022) sidestep the assumption of knowing the group labels on train data, but still rely on tuning hyper-parameters using worst-group accuracy on validation, and thus, having group labels on validation data. In fact, Idrissi et al. (2021) showed that ERM is a strong baseline when tuned with worst-group accuracy on validation.

Lee et al. (2022) explore the setting where they do not necessarily require group labels on validation data, but their method implicitly relies on the presence of sufficiently many minority examples in the validation set such that different prediction heads would disagree on those examples to choose the most reliable classifier.

Recent works Nam et al. (2022) and Sohoni et al. (2021) explore the setting where the group information is available on a small subset of the data (e.g. on the validation set), and the goal is to use the available data optimally, both to train the model and to tune the hyper-parameters. These methods use semi-supervised learning to extrapolate the available group labels to the rest of the training data. We consider this same setting with $\text{DFR}^{\text{Val}}_{\text{Tr}}$, where we use the validation data to retrain the last layer of the model.

C.2 DFR variations

Besides $\text{DFR}^{\text{Tr}}_{\text{Tr}}$ and $\text{DFR}^{\text{Val}}_{\text{Tr}}$ described in Section 6, we additionally consider $DFR^{Tr}_{Tr\text{-}NM}$ (NM stands for “No Minority"): we use a random group-balanced subset of the train data as $\hat{\mathcal{D}}$, but remove the

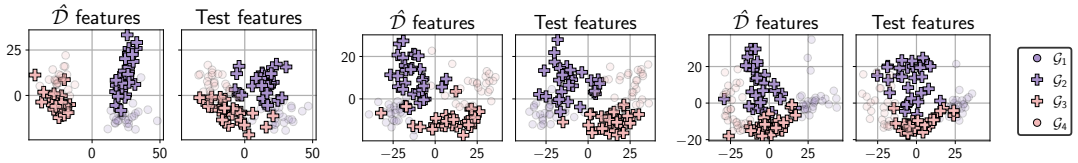

(a) $\text{DFR}^{\text{Tr}}_{\text{Tr}}$ (b) $\text{DFR}^{\text{Val}}_{\text{Tr}}$ (c) $\text{DFR}^{\text{Tr}}_{\text{Tr-NM}}$

Figure 8: **DFR Variations.** Visualization of the features extracted from the reweighting dataset $\hat{D}$ and the test data for different variations of DFR on the Waterbirds data. We show projections of the 2048-dimensional features on the top-2 principal components extracted from $\hat{D}$. With $\text{DFR}^{\text{Val}}_{\text{Tr}}$ and $\text{DFR}^{\text{Tr}}_{\text{Tr-NM}}$, the distribution of the features for the minority groups $\mathcal{G}_2$ and $\mathcal{G}_3$ does not change between the reweighting and test data, while with $\text{DFR}^{\text{Tr}}_{\text{Tr}}$ we see significant distribution shift.

minority groups ($\mathcal{G}_2, \mathcal{G}_3$ on Waterbirds and $\mathcal{G}_4$ on CelebA) from the data $\mathcal{D}$ used to train the feature extractor.

We compare different DFR versions in Table 9. All three DFR variations obtain results competitive with state-of-the-art Group DRO results on the Waterbirds data. On CelebA, $\text{DFR}^{\text{Val}}_{\text{Tr}}$ and $\text{DFR}^{\text{Tr}}_{\text{Tr-NM}}$ match Group DRO, while $\text{DFR}^{\text{Tr}}_{\text{Tr}}$ performs slightly worse, but still on par with JTT. In particular, *$\text{DFR}^{Tr}_{Tr\text{-}NM}$ matches the state-of-the-art Group DRO by using the same data to train and tune the model*. Notably, $\text{DFR}^{\text{Tr}}_{\text{Tr-NM}}$ achieves these results with the features extracted by the network trained *without seeing any examples from the minority groups*! Even without minority groups, ERM models extract the core features sufficiently well to achieve state-of-the-art results on the image classification benchmarks.

On the NLP datasets, $\text{DFR}^{\text{Val}}_{\text{Tr}}$ outperforms the other varations, but in all cases all DFR variations significantly improve performance compared to the base model. Notably, on CivilComments the no minority version group of the dataset only retains the toxic comments which mention the protected identities and non-toxic comments which do not mention these identities. As a result, the base model only achieves 8.4% worst group performance! $\text{DFR}^{\text{Tr}}_{\text{Tr-NM}}$ is still able to recover 66.5% worst group accuracy using the features extracted by this model.

C.3 Why is $\text{DFR}^{\text{Tr}}_{\text{Tr-NM}}$ better than $\text{DFR}^{\text{Tr}}_{\text{Tr}}$?

Let us consider the second stage of $\text{DFR}^{\hat{\mathcal{D}}}_{\mathcal{D}}$, where we fix the feature encoder $f(\cdot)$, and train a logistic regression model $\mathcal{L}$ on the dataset $f(\hat{\mathcal{D}})$, where by $f(\hat{\mathcal{D}})$ we denote the dataset with labels from the reweighting dataset $\hat{\mathcal{D}}$ and features from $\hat{\mathcal{D}}$ extracted by f. We then evaluate the logistic regression model $\mathcal{L}$ on the features extracted from the test data, $f(\mathcal{D}_{\text{Test}})$.

Let us use $\hat{\mathcal{M}}$ to denote a minority group in the reweighting dataset $\hat{\mathcal{D}}$, and $\mathcal{M}^{\text{Test}}$ to denote the same minority group in the test data. For $\text{DFR}^{\text{Tr}}_{\text{Tr-NM}}$ and $\text{DFR}^{\text{Val}}_{\text{Tr}}$, the model f is trained without observing any data from $\hat{\mathcal{M}}$ or $\mathcal{M}^{\text{Test}}$. Assuming the datapoints in $\hat{\mathcal{M}}$ and $\mathcal{M}^{\text{Test}}$ are iid samples from the same distirbution, the distribution of features in $f(\hat{\mathcal{M}})$ and $f(\mathcal{M}^{\text{Test}})$ will also be identical.

On the other hand, with $\text{DFR}^{\text{Tr}}_{\text{Tr}}$, the minority group datapoints $\hat{\mathcal{M}}$ are used to train the feature extractor f. In this case, we can no longer assume that the distribution of features $f(\hat{\mathcal{M}})$ will be the same as the distribution of $f(\mathcal{M}^{\text{Test}})$. Consequently, in $\text{DFR}^{\text{Tr}}_{\text{Tr}}$, the logistic regression model $\mathcal{L}$ will be evaluated under *distribution shift*, which makes the problem much more challenging and leads to inferior performance of $\text{DFR}^{\text{Tr}}_{\text{Tr}}$ on the Waterbirds data. We verify this intuition in Figure 8, where we visualize the feature embeddings for the reweighting dataset $\hat{D}$ and the test data. We see that as we predicted, the distribution of the minority group features coincides between $\hat{\mathcal{D}}$ and test data for $\text{DFR}^{\text{Tr}}_{\text{Tr-NM}}$ and $\text{DFR}^{\text{Val}}_{\text{Tr}}$, while $\text{DFR}^{\text{Tr}}_{\text{Tr}}$ shows significant distribution shift.

What $\hat{\mathcal{D}}$ should be used in practice? In Table 9, the best performance is achieved by $\text{DFR}^{\text{Tr}}_{\text{Tr-NM}}$ and $\text{DFR}^{\text{Val}}_{\text{Tr}}$, which retrain the last layer on data that was not used in training the feature extractor. In practice, we recommend collecting a group-balanced validation set, which can be used both to tune the hyper-parameters and re-train the last layer of the model, as we do in $\text{DFR}^{\text{Val}}_{\text{Tr}}$.

C.4 RELATION TO TRANSFER LEARNING

Algorithmically, DFR is a special case of transfer learning, where $\mathcal{D}$ serves as the source data, and $\hat{\mathcal{D}}$ is the target data (Sharif Razavian et al., 2014). However, the motivation of DFR is different from that of standard transfer learning: in DFR we are trying to correct the behavior of a pretrained model, and reduce the effect of spurious features, while in transfer learning the goal is to learn general features that generalize well to diverse downstream tasks. For example, we can use DFR to reduce the reliance of ImageNet-trained models on the background or texture and improve their robustness to covariate shift (see Section 7), while in standard transfer learning we would typically use a pretrained model as initialization or a feature extractor to learn a good solution on a *new dataset*. In the context of spurious correlations, one would not expect DFR to work as well as it does: the only reason DFR is successful is because, contrary to conventional wisdom, *neural network classifiers are in fact learning substantial information about core features, even when they seem to rely on spurious features to make predictions*. Moreover, in Appendix Table 6 we show that transfer learning with features learned ImageNet does not work nearly as well as DFR on the spurious correlation benchmarks.

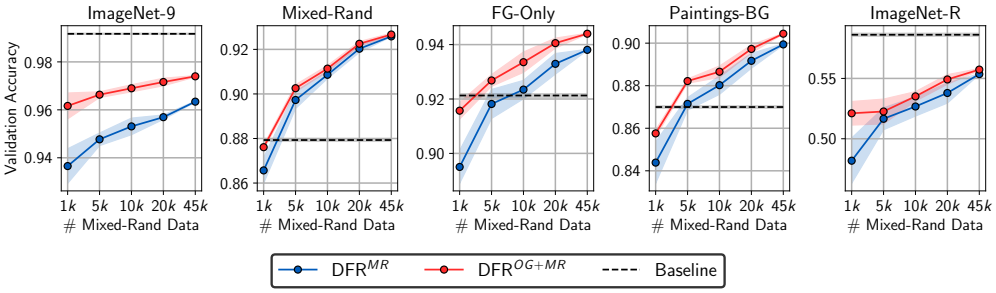

Figure 9: **ImageNet background reliance (VIT-B-16).** Performance of DFR trained on MixedRand data and MixedRand + Original data on different ImageNet-9 validation splits. All methods use an VIT-B-16 feature extractor trained on ImageNet21k and finetuned on ImageNet. DFR can reduce background reliance with a minimal drop in performance on the Original data. See Figure 3 for analogous results with a ResNet-50 feature extractor.

D Details: ImageNet Background Reliance

Here we provide details on the experiments on background reliance in Section 7.1 and additional evaluations verifying the main results.

Data. We use the ImageNet-9 dataset (Xiao et al., 2020). To test whether our models can generalize to unusual backgrounds, we additionally generate *Paintings-BG* data shown in Figure 11. For the Paintings-BG data we use the Original images and segmentation masks for ImageNet-9 data provided by Xiao et al. (2020), and combine them with random paintings from Kaggle's `painter-by-numbers` dataset available at kaggle.com/c/painter-by-numbers/ as backgrounds. For the ImageNet-R dataset (Hendrycks et al., 2021), we only use the images that fall into one of the ImageNet-9 categories, and evaluate the accuracy with respect to these categories. We show examples of images from different dataset variations in Figure 11.

Base model hyper-parameters. We use a ResNet-50 model pretrained on ImageNet and a VIT-B-16 model pretrained on ImageNet-21k and finetuned on ImageNet. The ResNet-50 model is imported from the `torchvision` package: `torchvision.models.resnet50(pretrained=True)`. The VIT-B-16 model is imported from the `lukemelas/PyTorch-Pretrained-ViT` package available at github.com/lukemelas/PyTorch-Pretrained-ViT; we use the command: `ViT('B_16_imagenet1k', pretrained=True)` to load the model. To extract the embeddings, we remove the last linear classification layer from each of the models. We preprocess the data using the `torchvision.transforms` paclage `Compose([ Resize(resize_size), CenterCrop(crop_size), ToTensor(), Normalize([0.485, 0.456, 0.406], [0.229, 0.224, 0.225])])`, where `(resize_size, crop_size)` are equal to (256, 224) for the ResNet-50 and (384, 384) for the VIT-B-16. We do not apply any data augmentation.

DFR details. We Train DFR on random subsets of the Mixed-Rand train data of different sizes (DFR^{MR}) or combinations of the Mixed-Rand and Original data (DFR$^{\text{OG+MR}}$). For DFR$^{\text{OG+MR}}$ we use the same number of Original and Mixed-Rand datapoints in all experiments. As the full ImageNet-9 contains $50k$ datapoints, we train the logistic regression on GPU with a simple implementation in PyTorch (Paszke et al., 2017). We then preprocess the embeddings to have zero mean and unit standard deviation using the standard scaler `sklearn.preprocessing.StandardScaler` from the `scikit-learn` package. In each case, we compute the preprocessing statistics on the reweighting data used to train the last layer. For the experiments in this section we use ℓ_2 regularization (as the number of datapoints is large relative to the number of observations, we do not have to use ℓ_1). We set the regularization coefficient λ to be 100 and train the logistic regression model with the loss $\sum_{x,y\in\mathcal{D}'} L(y, wx+b) + \frac{\lambda}{2}\|w\|^2$, where $L(\cdot,\cdot)$ is the cross-entropy loss. We use full-batch SGD with learning rate 1 and no momentum to train the model for 1000 epochs. We did not tune the λ parameter or SGD hyper-parameters.

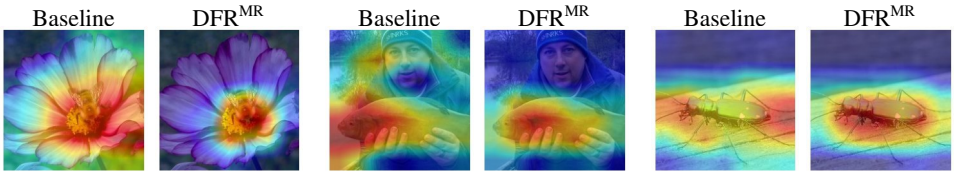

Figure 10: GradCAM visualizations of the features used by the baseline model and DFR^{MR} on ImageNet-9.

Results for VIT-B-16. We report the results for the VIT-B-16 base model in Figure 9. The results are generally analogous to the results for ResNet-50: it is possible to significantly reduce the reliance of the model on the background by retraining the last layer with DFR. For the VIT, removing the background dependence hurts the performance on the Original data slightly, but greatly improves the performance on the images with unusual backgrounds (Mixed-Rand, FG-Only, Paintings-BG). Removing the background dependence does not improve the performance on ImageNet-R.

BG modification. For each test image we generate images with 7 modified backgrounds: MixRand (random Only-BG-T ImageNet-9 background, [1]), Paintings-BG, and constant black, white, red, green and blue backgrounds. Then, for each model from Section 7.1 we compute the percentage of the datapoints, on which changing the background with a fixed foreground does not change the predictions compared to the original image. We get 87.5% for the baseline model, 92.4% for DFR^{MR}and 93.1% for DFR^{OG+MR}, suggesting that the DFR^{MR} and DFR^{OG+MR} models are significantly more robust to modifying the background.

Prediction based on BG. Next, for each model we evaluate the percentage of test MixRand datapoints on which the model makes predictions that match the background class and not the foreground class. We get 14.8% for the baseline model, 11.2% for DFR^{MR} and 11.7% for DFR^{OG+MR}. The baseline model predicts the background class significantly more frequently than the DFR models.

GradCAM. Finally, to gain a visual intuition into the features used by DFR^{MR}and the baseline models, in Figure 10 we make GradCAM feature visualizations on three images from ImageNet-9. We use the `pytorch-grad-cam` package (Gildenblat & contributors, 2021) available at github.com/jacobgil/pytorch-grad-cam. While the baseline model uses the background context, the DFR^{MR} features are more compact and focus on the target object, again suggesting that DFR reduces the reliance on the background information.

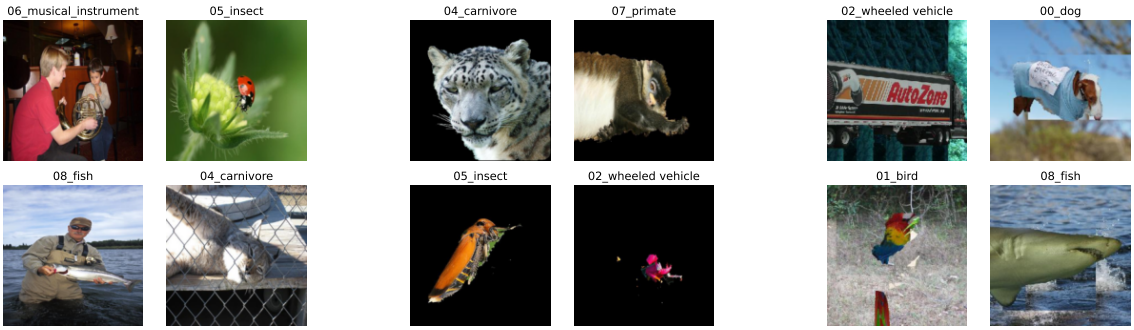

(a) IN-9 Original (Xiao et al., 2020) (b) IN-9 FG-Only (Xiao et al., 2020) (c) IN-9 Mixed-Rand (Xiao et al., 2020)

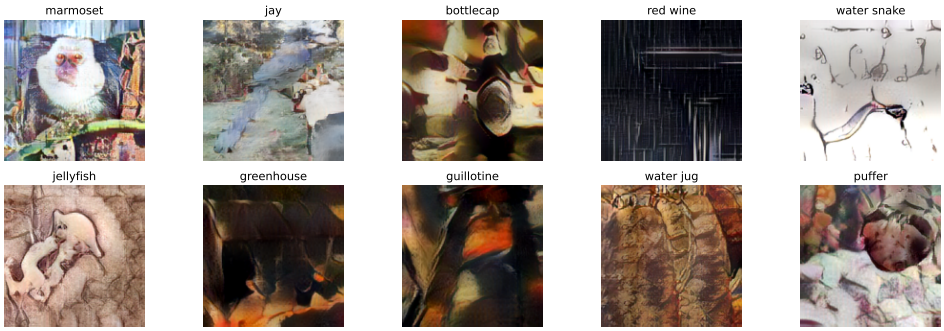

(d) Stylized ImageNet (Geirhos et al., 2018)

(e) ImageNet-R (Hendrycks et al., 2021)

(f) ImageNet-9, Paintings-BG (ours)

Figure 11: **ImageNet variations.** Examples of datapoints from the ImageNet variations used in the experiments.

E DETAILS: IMAGENET TEXTURE BIAS DETAILS

Here we provide details on the experiments on texture bias in Section 7.

Data. We generate the stylized ImageNet (SIN) data following the instructions at github.com/rgeirhos/Stylized-ImageNet (Geirhos et al., 2018). For evaluation, we use ImageNet-C (Hendrycks & Dietterich, 2019) and ImageNet-R datasets (Hendrycks et al., 2021). For ImageNet-C we report the average performance across all 19 corruption types and 5 corruption intensities. We show examples of stylized ImageNet images in Figure 11.

Base model hyper-parameters. We use the same ResNet-50 and VIT-B-16 models as described in Appendix D.

DFR details. We train DFR using the embeddings of the original ImageNet (IN), stylized ImageNet (SIN) and their combination (IN+SIN) as the reweighting dataset. We preprocess the base model embeddings by manually subtracting the mean and dividing by standard deviation computed on the reweighting data used to train DFR; we did not use `sklearn.preprocessing.StandardScaler` due to the large size of the datasets ($1.2M$ datapoints for IN and SIN; $2.4M$ datapoints for IN+SIN). We train the logistic regression for the last layer on a single GPU with a simple implementation in PyTorch. We use SGD with learning rate 1, no momentum, no regularization and batch size of 10^4 to train the model for 100 epochs. We tuned the batch size (in the range $\{10^3, 10^4, 10^5\}$) and picked the batch size that leads to the best performance on the ImageNet validation set (10^4). We did not tune the other hyper-parameters.

Results for VIT-B-16. We report the results for the VIT-B-16 base model in Table 10. For this model, baselines trained from scratch on IN+SIN and SIN are not available so we only report the results for the standard model trained on ImageNet21k and finetuned on ImageNet; for DFR we report the results using IN+SIN as the reweighting dataset. Despite the large-scale pretraining on ImageNet21k, we find that we can still improve the shape bias ($36\% \rightarrow 39.9\%$) as well as robustness to ImageNet-C corruptions ($49.7\% \rightarrow 52\%$ Top-1 accuracy). On the original ImageNet and ImageNet-R the performance of DFR is similar to that of the baseline model.

Detailed texture bias evaluation. To provide further insight into the texture bias of the models trained with DFR, in Figure 12 we report the fraction of shape and texture decisions for different classes following Geirhos et al. (2018). We produce the figure using the `modelvshuman` codebase available at github.com/bethgelab/model-vs-human (Geirhos et al., 2021). We report the results for both DFR models and models trained from scratch on IN, SIN and IN+SIN as well as the ShapeResNet-50 model and humans (results from Geirhos et al. (2018)). When trained on the same data, models trained from scratch achieve a higher shape bias than DFR models, but DFR can still significantly improve the shape bias compared to the base model trained on IN.

Detailed ImageNet-C results. In Figure 13, we report the Top-1 accuracy for DFR models and models trained from scratch on IN, SIN and IN+SIN on individual ImageNet-C datasets. We use the ResNet-50 base model. The model trained from scratch on IN+SIN provides the best robustness across the board, but DFR trained on IN+SIN also provides an improvement over the baseline RN50(IN) model on many corruptions.

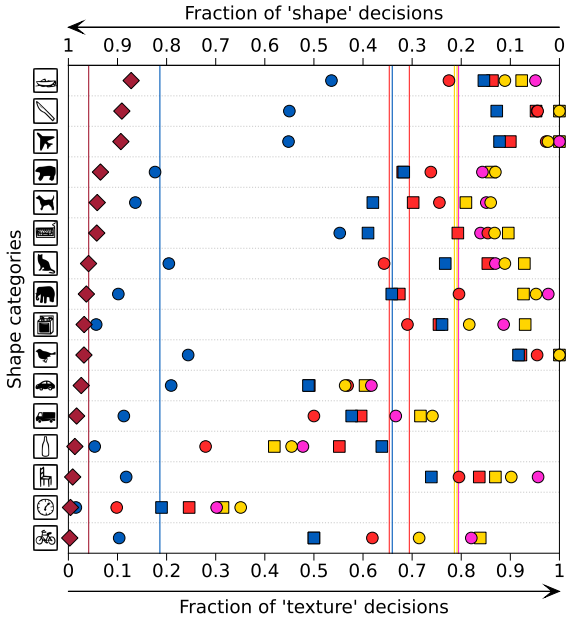

Figure 12: **Shape-texture bias report.** Detailed report of the shape-texture bias generated using the `model-vs-human` codebase (`https://github.com/bethgelab/model-vs-human`) (Geirhos et al., 2021). The plot shows the fraction of the decisions made based on shape and texture information respectively on examples with conflicting cues (Geirhos et al., 2018). The brown diamonds (◇) show human predictions and the circles (○) show the performance of ResNet-50 models trained on different datasets: ImageNet (IN, yellow), Stylized ImageNet (SIN, blue), ImageNet + Stylized ImageNet (IN+SIN, red), ImageNet + Stylized ImageNet Finetuned on ImageNet (IN+SIN→IN, pink); these models are provided in the `model-vs-human` codebase. For each dataset (except for IN+SIN→IN) we report the results for DFR using an ImageNet-trained ResNet-50 model as a feature extractor with squares □ of the corresponding colors. Reweighting the features in a pretrained model with DFR we can significatly increase the shape bias: DFR trained on SIN (blue squares) virtually matches the shape bias of the model trained from scratch on IN+SIN (red circles). However, the model trained just on SIN (blue circles) from scratch still provides a significantly higher shape bias, that we cannot match with DFR.

Method	**Training Data**	**Shape bias (%)**	**Top-1 Acc (%) / Top-5 Acc (%)**		
			ImageNet	ImageNet-R	ImageNet-C
VIT-B-16	IN21k + IN	36	79.2/95.0	29.1/42.0	49.7/69.3
DFR	IN+SIN	39.9	79.7/94.5	29.0/41.4	52.0/71.0

Table 10: **Texture-vs-shape bias results for VIT-B-16.** Shape bias, top-1 and top-5 accuracy on ImageNet validation set variations for VIT-B-16 pretrained on ImageNet21k and finetuned on ImageNet and DFR using this model as a feature extractor and reweighting the features on combined ImageNet and Stylized ImageNet datasets. By retraining just the last layer with DFR, we can increase the shape bias compared to the feature extractor model and improve robustness to covariate shift on ImageNet-C.

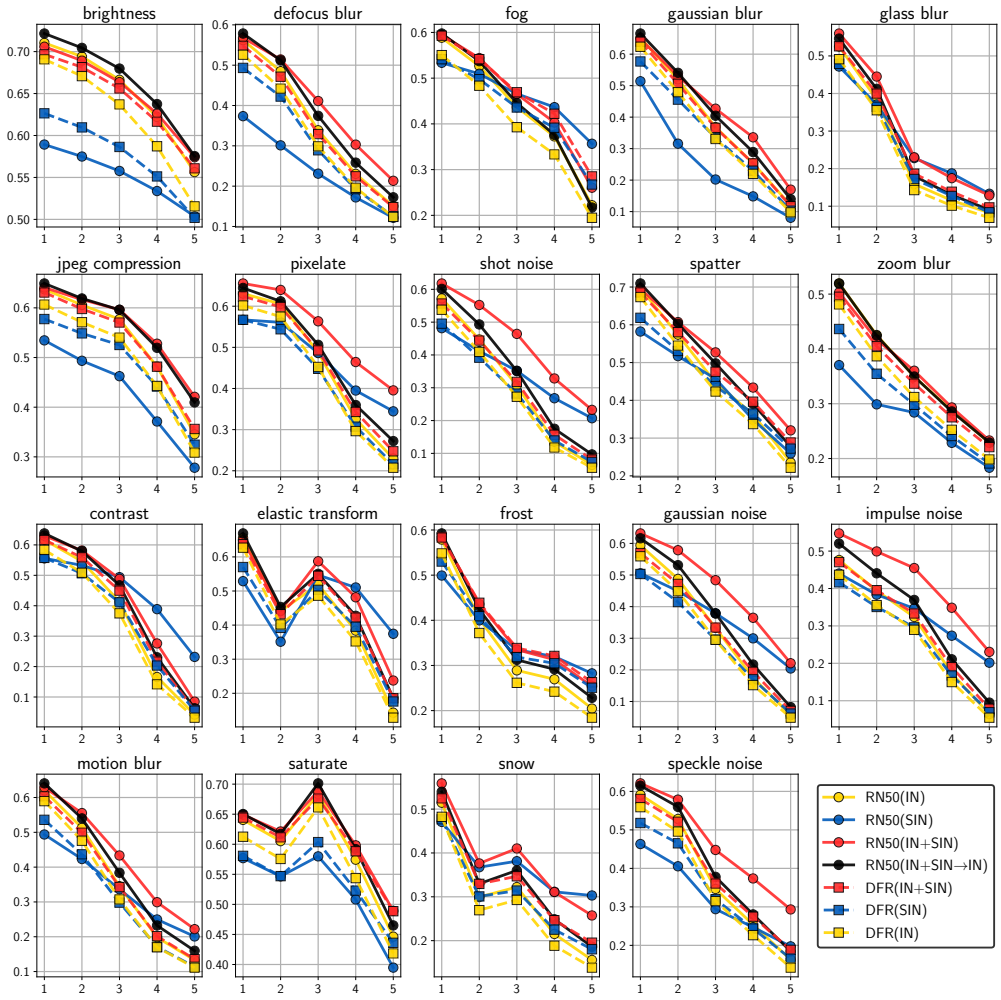

Figure 13: **ImageNet-C results.** Results of ResNet-50 models trained on different ImageNet variations (shown in circles) and DFR using an ImageNet-trained ResNet-50 model as a feature extractor on ImageNet-C and ImageNet-R datasets. Each panel corresponds to a different corruption, and the horizontal axis represents the corruption intensity. Retraining the last layer on ImageNet-Stylized (DFR(SIN), red squares) improves robustness to ImageNet-C corruptions compared to the base model (RN50(IN), blue circles), but does not match the robustness of a model trained from scratch on SIN or IN+SIN.

F FURTHER DISCUSSION

Spurious correlations and representation learning. Prior work has often associated poor robustness to spurious correlations with the quality of *representations* learned by the model (Arjovsky et al., 2019; Bahng et al., 2020; Ruan et al., 2021) and suggested that the entire model needs to be carefully trained to avoid relying on spurious features (e.g. Sagawa et al., 2019; Idrissi et al., 2021; Liu et al., 2021; Zhang et al., 2022; Sohoni et al., 2021; Pezeshki et al., 2021; Lee et al., 2022). Our work presents a different view: *representations learned with standard ERM even without seeing any minority group examples are sufficient to achieve state-of-the-art performance on popular spurious correlation benchmarks*. The issue of spurious correlations is not in the features extracted by the models (though the representations learned by ERM can be improved (e.g., Hermann & Lampinen, 2020; Pezeshki et al., 2021)), but in the weights assigned to these features. Thus we can simply re-weight these features for substantially improved robustness.

Practical advantages of DFR. DFR is extremely simple, cheap and effective. In particular, DFR has only one tunable hyper-parameter — the strength of regularization of the logistic regression. Furthermore, DFR is highly robust to the choice of base model, as we demonstrate in Appendix Table 8, and does not require early stopping or other highly problem-specific tuning such as in Idrissi et al. (2021) and other prior works. Moreover, as DFR only requires re-training the last linear layer of the model, it is also extremely fast and easy to run. For example, we can train DFR on the $1.2M$-datapoint Stylized ImageNet dataset in Section 7 on a single GPU in a matter of minutes, after extracting the embeddings on all of the datapoints, which only needs to be done once. On the other hand, existing methods such as Group DRO (Sagawa et al., 2019) require training the model from scratch multiple times to select the best hyper-parameters, which may be impractical for large-scale problems.

On the need for reweighting data in DFR. Virtually all methods in the spurious correlation literature, even the ones that do not explicitly use group information to train the model, use group-labeled data to tune the hyper-parameters (we discuss the assumptions of different methods in prior work in Appendix C.1). If a practitioner has access to group-labeled data, we believe that they should leverage this data to find a better model instead of just tuning the hyper-parameters. Finally, we note that DFR can be easily combined with methods that automatically estimate group labels (e.g. Liu et al., 2021; Creager et al., 2021; Sohoni et al., 2021): we can retrain the last layer using these estimated labels instead of ground truth.

Future work. There are many exciting directions for future research. DFR largely reduces the issue of spurious correlations to a linear problem: how do we train an optimal linear classifier on given features to avoid spurious correlations? In particular, we can try to avoid the need for a balanced reweighting dataset by carefully studying this linear problem and only using the features that are robustly predictive across all of the training data. We can also consider other types of supervision, such as saliency maps (Singla & Feizi, 2021) or segmentation masks to tell the last layer of the model what to pay attention to in the data. Finally, we can leverage better representation learning methods (Pezeshki et al., 2021), including self-supervised learning methods (e.g. Chen et al., 2020; He et al., 2021), to further improve the performance of DFR.